Physics of light mesons in a quark model with confinement

G. V. Efimov and M. A. Ivanov

Joint Institute for Nuclear Research, Dubna

Fiz. Elem. Chastits At. Yadra **20**, 1129–1184 (September–October 1989)

A relativistic quark model with confinement is proposed on the basis of certain assumptions about hadronization and confinement. Hadrons are regarded as collective variables that arise as a result of quark–gluon interactions. The confinement mechanism is based on averaging intermediate quark states over the nontrivial QCD vacuum. It is shown that at small momenta the model reproduces the low-energy relations of chiral theory. Numerous effects of the low-energy physics of light mesons are treated in the framework of the model. Thus, calculations are made of the widths of strong, weak, and electromagnetic decays of mesons, of form factors and slope parameters, etc. The results obtained are in good agreement with the experimental data.

INTRODUCTION

Considerable efforts are currently being made in order to obtain a description of low-energy hadron physics from the fundamental ideas of QCD (see, for example, the review of Ref. 1). The main difficulty is, of course, that QCD perturbation theory, based on asymptotic freedom, is not valid at large distances or at low energies. No answers have yet been found to fundamental problems such as hadronization, i.e., the formation of colorless hadrons as a result of quark–gluon interactions, and confinement, i.e., the absence of quarks and gluons in the observed hadron spectrum.

This situation has led to the development of various approaches and models that, on the one hand, are based on ideas taken from QCD, while, on the other, they use certain assumptions in order to calculate the properties of hadronic interactions at low energies.

It appears that the closest connection with QCD is currently achieved by the QCD sum-rule method,[2] which is based on the duality principle. This method makes it possible to relate chromodynamic quantities to hadronic properties. Nonperturbative effects are determined by the nontrivial vacuum structure of QCD and are taken into account phenomenologically by means of quark and gluon condensates. The agreement with experiment is impressive. However, the problem of confinement is in no way attacked.

Existing bag models,[3] based on a quite definite picture of confinement, have made it possible to describe a number of static properties of hadrons (masses, magnetic moments, widths of radiative transitions, etc.). The systematic description of hadronic interactions in these approaches is a very difficult task.

Great popularity has been achieved by approaches[4–11] that are dubbed QCD bosonization and are regarded as the low-energy limit of QCD, and in which a particular understanding of the mechanism of formation of hadronic states in QCD is formulated. The aim of such approaches is to obtain phenomenological chiral Lagrangians that describe low-energy hadronic physics.

In the studies of Refs. 4–7, hadron fields appear as the phases of chiral transformations, and the constants which appear in front of the corresponding terms of the nonlinear chiral Lagrangian can, in principle, be related to chromodynamic quantities (Λ_{QCD}, values of vacuum condensates, etc.). The hadrons are described by local fields, and their internal quark structure is in no way manifested.

More heuristic approaches, based on the ideas of Nambu and Jona-Lasinio,[8] proceed from the idea of obtaining chiral dynamics from effective four-fermion quark Lagrangians. In this approach, one can trace the formation of hadrons as bound states in quark systems. Moreover, the spontaneous breaking of chiral symmetry finds here a natural dynamical explanation. Such an approach leads to phenomenological meson Lagrangians in which the meson vertices are determined by quark loops. Allowance for and parametrization of only the principal divergences of these loops and also of the terms quadratic in the meson momenta leads to a good description of the experimental data at low energies for the basic properties of the mesons.[11] In the cited studies, the problem of quark confinement is not discussed, and, as a consequence, a possibility does not exist for the description of more subtle effects associated with manifestation of the quark structure of hadrons.

It is now widely accepted that at low energies the complicated structure of the QCD vacuum plays an important part. Very popular and well known in this respect are instanton solutions.[12–17] By means of them it is possible to explain some features of the low-energy physics[13,14] and to obtain a foundation of the bag model.[20] Instanton contributions explained the values of the gluon and quark condensates that are used in the method of QCD sum rules.[2] However, the instanton vacuum does not ensure quark confinement.

Vacuum self-dual gluon fields, which lead to confinement of all colored objects, are also known. We have here fields with constant field strengths[12,15] and stochastic gluon fields.[16] The investigation of the properties of colorless objects in such a vacuum is an extremely difficult problem. Moreover, methods have not yet been developed that permit the use, for example, of the propagators of quarks in external confining fields[17] in low-energy phenomenology.

Thus, we see that basic ideas of quark–hadron physics such as confinement, hadronization, and low-energy phenomenology have not yet been unified into a theory of hadronic interactions at low energies. In this paper, we shall formulate a model in which an attempt is made to relate these ideas. We propose a relativistic quark model with phenomenological allowance for confinement. This model makes it possible to describe the quark structure of hadrons (both mesons and baryons) at low energies from a unified point of view. The model, which we shall call the Quark Confinement Model (QCM), is based on the following physical picture. It is as-

 0090-4759/89/050479-25$04.40

sumed that there exist vacuum gluon configurations that ensure confinement of colored objects. Hadrons, as colorless states, appear in the form of collective excitations in quark–gluon interactions. In this point, we follow the ideas of Ref. 10. The hadron–hadron interactions are described by means of corresponding quark diagrams, averaged over the gluon vacuum fields. The hypothesis of quark confinement means that such averaging ensures the absence of constituent quarks as physical particles in the observable hadron spectrum.

At small momentum transfers, the QCM reproduces the low-energy theorems of current algebra but, in contrast to phenomenological chiral Lagrangians, enables one to take into account the quark structure of the hadron–hadron vertices. Thus, the QCM permits a description of not only the decay constants of the hadrons but also more subtle properties of them—slope parameters, form factors, etc.

The paper is arranged as follows. Section 1 describes the scheme of the transition to colorless collective variables in the generating functional of QCD. The conditions for the appearance of mesonic states in colorless quark systems are discussed. An equivalent formulation of the proposed hadronization scheme that can be readily generalized to the case of many-quark states is proposed.

In Sec. 2 we formulate requirements on the procedure for the averaging over the vacuum gluon configurations of the quark diagrams that describe the hadron–hadron interactions. The most important requirements are: first, the confinement postulate, which reduces to the requirement that there be no cuts corresponding to production of quarks in the matrix elements of physical processes, and, second, the requirement of ultraviolet convergence of the Feynman integrals. The connection between the quark confinement postulate and the hypothesis of quark–hadron duality is discussed.

In Sec. 3 we formulate the rules for calculation of the higher approximations for the matrix elements of physical processes. These rules are based on the $1/N_c$ expansion and lead to the appearance in the matrix elements of cuts associated with allowance for intermediate hadronic states.

In Sec. 4 we discuss questions related to the fulfillment of gauge and chiral invariance in the QCM, and we derive an anomalous Ward identity. The parameters of the QCM are determined by means of a fit to the main decays of the light mesons. The connection between the results of the model and the well-known low-energy relations (Goldberger–Treiman relation, Adler anomaly and PCAC, universality of vector mesons, etc.) is shown. The breaking of the group SU_3 is discussed, and the main decays of strange mesons are calculated.

In Sec. 5 we calculate the slope parameters in Dalitz decays ($P\to\gamma l^+l^-$, $V\to Pl^+l^-$), the pion form factor in the Euclidean and pseudo-Euclidean domains, the ratio of the axial and vector form factors in the decay $\pi^-\to ev\gamma$, the electromagnetic radii of kaons, and the parameters of Kl_3 decay. The results obtained are in agreement with the experimental data. The part played by the quark structure of the hadrons in the calculation of these quantities is shown.

In Sec. 6 we consider scalar 0^{++} mesons and discuss their role in low-energy meson physics. Using the Adler condition for the $\pi\pi\to\pi\pi$ and $\pi\gamma\to\pi\gamma$ amplitudes, we determine the parameters that characterize the scalar mesons as two-quark systems. We calculate the s-wave $\pi\pi$ scattering lengths, the pion polarizability, and the strong and electromagnetic decays of scalar mesons. We compare the results obtained with existing experimental data and with other approaches.

Section 7 is devoted to the study of nonleptonic decays of kaons. As effective Hamiltonians of the weak interactions that describe $\Delta S=1$ transitions, we use the Hamiltonians obtained in the standard Weinberg–Salam model with allowance for QCD corrections.[21]

We calculate the widths of the decays $K\to\pi\pi$, $\gamma\gamma$. We make a comparison with experiment and with the results of other approaches.

1. HADRONIZATION AND HYPOTHESIS ABOUT THE QCD VACUUM

As we said in the Introduction, we shall understand the mechanism of hadronization as a transition to collective variables in the generating functional of QCD. Following Refs. 8 and 9, we demonstrate the procedure of hadronization by the example of the transition from quark–gluon variables to hadron variables in the vacuum QCD functional.

The QCD functional integral is expressed in the standard form

$$Z_{\rm QCD}=\int\delta q\int\delta\bar q\int\delta B\delta\left(\partial^\mu B_\mu\right)\Delta_L[B]\,e^{iS[B]},\qquad(1)$$

where $\Delta_L[B]$ is the corresponding Faddeev–Popov determinant associated with the choice of the Lorentz gauge ($\partial^\mu B_\mu=0$):

$$\begin{aligned}&S[B]=\int dx\,\mathcal{L}_{\rm QCD}(x),\\ &\mathcal{L}_{\rm QCD}(x)=\frac{1}{8g^2}\,\mathrm{tr}\,F_{\mu\nu}^2+\bar q\left(i\hat\partial+\hat B\right)q,\\ &F_{\mu\nu}=\partial_\mu B_\nu-\partial_\nu B_\mu+[B_\nu,\ B_\mu],\\ &B_\mu=B_\mu^a\gamma^\mu t^a,\quad \mathrm{tr}\,(t^at^b)=2\delta^{ab},\end{aligned}\qquad(2)$$

where t_a ($a=1,\ldots,N_c^2-1$) are the generators of the group $SU(N_c)$, B_μ^a are the gluon fields, and $q(x)=q_f^a(x)$ are the quark fields.

The Lagrangian (2) is invariant with respect to the transformations

$$\begin{aligned}&B_\mu\to B_\mu^\omega=\omega B_\mu\omega^{-1}+(\partial_\mu\omega)\,\omega^{-1},\\ &q\to q^\omega=\omega q.\end{aligned}$$

In accordance with the hypothesis of a nontrivial structure of the vacuum, we decompose the gluon field B_μ^a into vacuum configurations $B_{\mu\rm vac}^a(x,\sigma_{\rm vac})$ characterized by the set of parameters $\{\sigma\}$, and quantum fluctuations $b_a^\mu(x)$. A detailed decomposition was made in the study of Ref. 14, and is as follows. We represent the field $B_\mu(x)$ in the form

$$B^\mu(x)=\left(B_{\rm vac}^\mu(x,\ \sigma_{\rm vac})+b^\mu(x)\right)^{\omega(x)}.$$

For the field $b^\mu(x)$, we choose the Lorentz gauge in the external field $B_{\rm vac}^\mu(x,\sigma_{\rm vac})$:

$$D_\mu[B_{\rm vac}]\,b^\mu(x)=0,$$

where $D_\mu[B_{\rm vac}]$ is the covariant derivative. We insert unity in the functional integral[22]:

$$\int \delta b \int \delta\omega \int d\sigma_{\text{vac}} \delta\left(B-(B_{\text{vac}}+b)^{\omega}\right) \delta$$

$$\times\left(D_{\mu}\left[B_{\text{vac}}\right] b^{\mu}\right) \Phi[B]=1.$$

Here, $\Phi[B]=\Phi[B^{\omega}]$ is determined by the given equation. After simple manipulations, we obtain

$$Z_{\text{QCD}}=\int \delta q \int \delta \bar{q} \int d\sigma_{\text{vac}}$$

$$\times \exp\left\{i \int dx\, \bar{q}\left(i\hat{\partial}+\hat{B}_{\text{vac}}\right) q\right\} W[J], \tag{3}$$

$$W[J]=\int \delta b \delta\left(D^{\mu}\left[B_{\text{vac}}\right] b_{\mu}\right) \Phi\left[B_{\text{vac}}+b\right]$$

$$\times \exp\left\{i \int dx \frac{1}{8g^2} \operatorname{tr} F_{\mu\nu}^2\left(B_{\text{vac}}+b\right)+i \int dx\, b_{\mu}^{a} J_{a}^{\mu}\right\}, \tag{4}$$

where $J_a^{\mu}=q\bar{\gamma}^{\mu} t^a q$ is the colored quark current. Recalling the definition of the connected Green's function of a gluon in the external field B_{vac},

$$G_{\mu_1 \ldots \mu_n}^{a_1 \ldots a_n}\left(x_1 \ldots x_n \mid B_{\text{vac}}\right)=\left.\frac{\delta^n \ln W[J]}{\delta J_{\mu 1}^{a 1}\left(x_1\right) \ldots \delta J_{\mu_n}^{a_n}\left(x_n\right)}\right|_{J=0},$$

we obtain

$$W[J]=\exp\left\{\sum_n \frac{1}{n!} \int dy_1 \ldots \int dy_n\, J_{\mu_1}^{a_1}\left(y_1\right) \ldots\right.$$

$$\left.\ldots J_{\mu_n}^{a_n}\left(y_n\right) G_{\mu_1 \ldots \mu_n}^{a_1 \ldots a_n}\left(y_1 \ldots y_n \mid B_{\text{vac}}\right)\right. . \tag{5}$$

Substituting (5) in (3), we finally obtain

$$\left.\begin{aligned} Z_{\text{QCD}} &= \int \delta q \int \delta \bar{q} \int d\sigma_{\text{vac}} \\ &\times \exp\left\{i \int dx\, \bar{q}\left(i\hat{\partial}+\hat{B}_{\text{vac}}\right) q+\sum_n L_n\right\}, \\ L_n &= \frac{1}{n!} \int dy_1 \ldots \int dy_n\, J_{\mu_1}^{a_1}\left(y_1\right) \ldots J_{\mu_n}^{a_n}\left(y_n\right) \\ &\times G_{\mu_1 \ldots \mu_n}^{a_1 \ldots a_n}\left(y_1 \ldots y_n \mid B_{\text{vac}}\right). \end{aligned}\right\} \tag{6}$$

It should be emphasized that the representation (6) is completely equivalent to the original expression (1). To make further advance, we must know the structure of the vacuum $d\sigma_{\text{vac}}$ and $B_{\text{vac}}(x, \sigma_{\text{vac}})$, and also the connected gluon Green's functions $G_{\{\mu\}}^{\{a\}}(x, B_{\text{vac}})$. Since all these problems are as yet unsolved, we make a number of assumptions about the structure of the QCD vacuum. These assumptions will provide the basis of the QCM.

We consider the term L_2 bilinear in the colored quark currents J_{μ}^{a} in (6); it is responsible for the formation of mesons. The dynamics of meson formation is determined by the behavior of the two-point gluon Green's function $G_{\mu_1 \mu_2}^{a_1 a_2}(x_1, x_2 \mid B_{\text{vac}})$. We shall assume that

$$G_{\mu_1 \mu_2}^{a_1 a_2}\left(x_1, x_2 \mid B_{\text{vac}}\right)=-i g_{\mu_1 \mu_2} \delta_{a_1 a_2} \delta\left(x_1-x_2\right) G_0. \tag{7}$$

This assumption is the basis of the Nambu–Jona-Lasinio model[8] and has been used in a number of studies.[9-11] We substitute the representation (7) in L_2 and go over to colorless quark currents by means of a Fierz transformation. We obtain

$$L_2=\frac{i}{2} \sum_{J_f=PVSA} c_J \int dx\, J_{Jf}(x) J_{Jf}(x). \tag{8}$$

Here

$$J_{Jf}(x)=\bar{q}(x) \Gamma_J \lambda_f q(x),$$

$$c_P=c_S=G_0,\ c_V=c_A=-1/2\, G_0,$$

$$\delta_P=\delta_S=1,\quad \delta_V=\delta_A=-1,$$

$\Gamma_J=I, \gamma^{\mu}, i\gamma^5, \gamma^{\mu}\gamma^5$ for $J=S, V, P, A$; λ_f are the Gell–Mann matrices of the group $SU_f(3)$.

We use the representation

$$\exp\left\{\pm \frac{i}{2} \int dx\, g^2 J^2(x)\right\}$$

$$=\int \delta M \exp\left\{\mp \frac{i}{2} \int dx\, M^2(x)+ig \int dx\, M(x) J(x)\right\}. \tag{9}$$

The next step is to interpret the field $M(x)$ as a colorless hadronic state with quantum numbers of the quark current $J(x)$. Thus, the hypothesis (7) leads to the appearance of the lowest nonets of pseudoscalar, vector, scalar, and axial-vector mesons, since only such quark currents are present in the representation (8).

Before we proceed further, we comment on the assumption (7). This ansatz should be regarded as a first approximation in the method of collective variables. We shall show how the next step can be made in the generalization of the assumption (7). We turn to L_2 in (6):

$$L_2=\frac{1}{2} \int dx_1 \int dx_2\, J_{\mu_1}^{a_1}(x_1)\, G_{\mu_1 \mu_2}^{\alpha_1 a_2}\left(x_1, x_2 \mid B_{\text{vac}}\right) J_{\mu_2}^{a_2}(x_2). \tag{10}$$

We assume for simplicity that

$$G_{\mu_1 \mu_2}^{a_1 a_2}\left(x_1, x_2 \mid B_{\text{vac}}\right)=-i g_{\mu_1 \mu_2} \delta_{a_1 a_2} G\left(x_1, x_2 \mid B_{\text{vac}}\right). \tag{11}$$

We substitute (11) in (10) and go over to colorless quark currents. Making the substitution $x_1=x+y/2$, $x_2=x-y/2$, we obtain

$$L_2=\frac{i}{2} \int dx \int dy \sum_{Jf} c_J J_{Jf}(x, y)\, G\left(x, y \mid B_{\text{vac}}\right) J_{Jf}(x, -y), \tag{12}$$

where

$$J_{Jf}(x, y)=q(x+y/2)\, \Gamma_J \lambda_f q(x-y/2).$$

We introduce an orthonormal system of functions

$$\left\{R_{nl}\left(y \mid B_{\text{vac}}\right)\right\} \quad (n, l=0, 1, 2, \ldots). \tag{13}$$

Here, the number l determines the orbital angular momentum, and n is the radial quantum number. For example, this system could take the form

$$R_{nl}\left(y \mid B_{\text{vac}}\right)=P_{nl}\left(y^2 \mid B_{\text{vac}}\right) T_{\mu_1 \ldots \mu_l}^{l}(y),$$

where $T_{\mu_1 \ldots \mu_l}(y)$ is a tensor completely symmetric with respect to the interchange $\mu_i \leftrightarrow \mu_j$ and for which

$$T_{\mu\mu\mu_3 \ldots \mu_l}^{l}(y)=0.$$

Strictly speaking, this system of functions (13) must be found by solving equations of Bethe–Salpeter or Schwinger–Dyson type for the bound states in the quark–antiquark system (see, for example, Ref. 23).

If we believe that the transition to the collective variables in the functional (6) is a transition to physical hadronic states, then the system (13) must satisfy conditions of the form

$$\int dy R_{nl}(y \mid B_{\text{vac}})\, G(x, y) \mid B_{\text{vac}})\, R_{n'l'}(y \mid B_{\text{vac}})$$
$$= \delta_{nn'}\delta_{ll'}(-)^l. \tag{14}$$

In this case, introducing the expansion

$$\left.\begin{aligned} J(x, y) &= \sum_{n, l} J_{nl}(x)\, R_{nl}(y \mid B_{\text{vac}}), \\ J_{nl}(x) &= \int dz\, J(x, -z)\, R_{nl}(z \mid B_{\text{vac}})\, G(x, z \mid B_{\text{vac}}) \end{aligned}\right\} \tag{15}$$

and substituting it in (12), we obtain

$$L_2 = \frac{\mathrm{i}}{2} \sum_{Jf} \sum_{nl} (-)^l c_J \int dx\, J^{nl}_{Jf}(x)\, J^{nl}_{Jf}(x). \tag{16}$$

Thus, the currents $J^{nl}_{Jf}(x)$ can describe mesons with all mesonic quantum numbers (arbitrary spin and all possible radial excitations).

We turn to our main hypothesis, i.e., to the representations (7) and (9). We substitute them in (6) and omit all higher terms L_n $(n \geqslant 3)$, and we obtain

$$Z^{(2)}_{\text{QCD}} = \int d\sigma_{\text{vac}} \int \delta q \int \delta\bar{q} \int \prod_{Jf} \delta M_{Jf} \exp\left[-\frac{\mathrm{i}}{2} \sum_{Jf} \delta_J M^2_{Jf}\right]$$
$$\times \exp\left\{\mathrm{i} \int dx\, \bar{q}\,[\mathrm{i}\hat{\partial} + \hat{B}_{\text{vac}} + M(x)]\, q\right\}. \tag{17}$$

Here

$$M(x) = \sum_{Jf} g_J M_{Jf}(x)\, \Gamma_J \lambda_f.$$

Integrating over the quark fields, we obtain

$$Z^{(2)}_{\text{QCD}} = \int \prod_{Jf} \delta M_{Jf} \exp\left\{-\frac{\mathrm{i}}{2} \int dx \sum_{Jf} \delta_J M^2_{Jf}\right\}$$
$$\times \int d\sigma_{\text{vac}} \exp\left\{-\sum_n \frac{\mathrm{i}^n}{n} \int dx_1 \ldots \int dx_n \right.$$
$$\left. \times \operatorname{tr}[M(x_1)\, S(x_1, x_2 \mid B_{\text{vac}}) \ldots M(x_n)\, S(x_n, x_1 \mid B_{\text{vac}})]\right\}, \tag{18}$$

where

$$S(x, y \mid B_{\text{vac}}) = (\mathrm{i}\hat{\partial}_x + \hat{B}_{\text{vac}}(x))^{-1}\, \delta(x - y).$$

Our next assumption is that the expression (18) can be written in the form

$$Z^{(2)}_{\text{QCD}} = \int \prod_{Jf} \delta M_{Jf} \exp\left\{-\frac{\mathrm{i}}{2} \sum_{Jf} \int dx\, \delta_J M^2_{Jf}\right\}$$
$$\times \exp\left\{-\sum_n \frac{\mathrm{i}^n}{n} \int dx_1 \ldots \int dx_n \int d\sigma_{\text{vac}} \right.$$
$$\left. \times \operatorname{tr}[M(x_1)\, S(x_1, x_2 \mid B_{\text{vac}}) \ldots M(x_n)\, S(x_n, x_1 \mid B_{\text{vac}})]\right\}. \tag{19}$$

This assumption means that at low energies the couplings between the quark loops through the vacuum gluon fields can be ignored. Averaging over the vacuum configurations $d\sigma_{\text{vac}}$ in (19) must lead to quark confinement. Assumptions about the measure $d\sigma_{\text{vac}}$ will be made in the next section.

The further program consists of separating the free Lagrangian describing fields M_J with masses m_J^2 and the Lagrangian of the interaction of these fields in the representation (19). This program is carried out in complete analogy with Refs. 8–11. In this way spontaneous breaking of the chiral symmetry occurs, the constituent quark acquires mass, and a Goldstone particle appears in the pseudoscalar channel. In this paper, we shall not dwell in detail on these questions, but merely show how the Lagrangian describing the bosonic fields M_J with masses m_J^2 arises in the representation (19).

In the sum (19), we separate the terms that are diagonal in the mesonic variables (for simplicity, we shall omit the flavor index f):

$$-\frac{\mathrm{i}}{2} \int dx_1 \int dx_2 \sum_J \delta_J M_J(x_1) \left[\delta(x_1 - x_2) \right.$$
$$\left. + \frac{N_c c_J}{(2\pi)^2} \Pi_J(x_1 - x_2)\right] M_J(x_2)$$
$$= -\frac{\mathrm{i}}{2} \sum_J \delta_J \int dp\, \tilde{M}_J(p) \left[1 + \frac{N_c c_J}{(2\pi)^2} \tilde{\Pi}_J(p^2)\right] \tilde{M}_J(p),$$

where

$$\left.\begin{aligned} \Pi_J(x_1 - x_2) &= \mathrm{i}(2\pi)^2 \delta_J \int d\sigma_{\text{vac}} \operatorname{tr}[\Gamma_J S(x_1, x_2 \mid B_{\text{vac}})\, \Gamma_J \\ &\quad \times S(x_2, x_1 \mid B_{\text{vac}})], \\ \tilde{\Pi}_J(p^2) &= \int dx\, \mathrm{e}^{\mathrm{i}px} \Pi_J(x). \end{aligned}\right\} \tag{20}$$

We represent $\tilde{\Pi}_J(p^2)$ in the form

$$\tilde{\Pi}_J(p^2) = \tilde{\Pi}^{\text{ren}}_J(p^2) + \tilde{\Pi}_J(m_J^2) + \tilde{\Pi}'_J(m_J^2)(p^2 - m_J^2)$$

and require fulfillment of the condition

$$1 + \frac{N_c c_J}{(2\pi)^2} \tilde{\Pi}_J(m_J^2) = 0. \tag{21}$$

In principle, Eq. (21) gives a connection between the mass spectrum m_J^2 of the mesons, the expansion coefficients of the total gluon Green's function (7) at large distances, and the universal confinement functions that arise on averaging over the measure $d\sigma_{\text{vac}}$ of the vacuum gluon field.

With allowance for Eq. (21), we go over in the representation (19) to the normalization

$$M_J(x) \to M_J(x) \left[-\frac{N_c c_J}{(2\pi)^2} \tilde{\Pi}'_J(m_J^2)\right]^{-1/2}$$

We have

$$Z^{(2)}_{\text{QCD}} = \int \prod_J \delta M_J$$
$$\times \exp\left\{\frac{\mathrm{i}}{2} \int dx \sum_J \delta_J M_J(x)(\Box - m_J^2) M_J(x)\right\}$$
$$\times \exp\left\{-\sum_n{}' \frac{\mathrm{i}^n}{n} \int dx_1 \ldots \int dx_n \int d\sigma_{\text{vac}} \right.$$
$$\left. \times \operatorname{tr}[M(x_1)\, S(x_1, x_2 \mid B_{\text{vac}}) \ldots M(x_n)\, S(x_n, x_1 \mid B_{\text{vac}})]\right\}, \tag{22}$$

where

$$M(x) = \sum_J \frac{\Gamma_J M_J(x)}{\sqrt{-\frac{N_c}{(2\pi)^2} \tilde{\Pi}'_J(m_J^2)}}.$$

The prime on the sum in (22) means that $\tilde{\Pi}^{\text{reg}}_J$ must be substituted in the quadratic terms diagonal in M_J.

The representation (22) does not contain in explicit

form G_0, which determines the behavior of the gluon propagator near $p^2 = 0$.

The generating functional $Z^{(2)}_{\text{QCD}}$ in (22), which determines the interactions of the mesons with each other through the quark loops, is the basis of our model. However, in practical work it is more convenient to use a different representation, which is completely equivalent to (22). We shall show that the functional $Z^{(2)}_{\text{QCD}}$ in (22) can be rewritten in the form

$$Z^{(2)} = \int \prod_J \delta M_J \int \delta q \int \delta \bar{q} \int d\sigma_{\text{vac}} \times \exp\left\{\frac{i}{2}\sum_J \delta_J \int dx\, M_J(x)(\Box - m_{0J}^2) M_J(x) + i\int dx\, \bar{q}(x)(i\hat{\partial} + \hat{B}_{\text{vac}})\, q(x) + \sum_J i g_{0J} \int dx\, M_J(x)\, \bar{q}(x)\, \Gamma_J q(x)\right\} \quad (23)$$

provided that the renormalization constant M_J of the meson wave function is zero.

To this end, we integrate (23) over the quark fields with the same assumptions about the action of the measure:

$$Z^{(2)} = \int \prod_J \delta M_J \exp\left\{\frac{i}{2}\int dx \sum_J \delta_J M_J(x)(\Box - m_{0J}^2) M_J(x)\right\} \times \exp\left\{-\sum_n \frac{i^n}{n}\int dx_1 \ldots \int dx_n \int d\sigma_{\text{vac}} \times \operatorname{tr}[M(x_1) S(x_1, x_2 \mid B_{\text{vac}}) \ldots M(x_n) S(x_n, x_1 \mid B_{\text{vac}})]\right\}. \quad (24)$$

Here,

$$M(x) = \sum_J g_{0J}\Gamma_J M_J(x).$$

Similarly, in (24) we separate the quadratic terms diagonal in M_J:

$$\frac{i}{2}\int dp\, \tilde{M}_J(p)(p^2 - m_0^2 - h_{0J}\tilde{\Pi}_J(p^2))\tilde{M}_J(p) = \frac{i}{2}\int dp\, \tilde{M}_J(p)(p^2 - m_J^2)\tilde{M}_J(p) Z_J^{-1} - \frac{i}{2}\int dp \tilde{M}_J(p) h_{0J}\tilde{\Pi}_J^{\text{reg}}(p^2)\tilde{M}_J(p),$$

where

$$h_{0J} = N_c g_{0J}^2/(2\pi)^2;$$
$$m_J^2 = m_{0J}^2 + h_{0J}\tilde{\Pi}_J(m_J^2);$$
$$Z_J^{-1} = 1 - h_{0J}\tilde{\Pi}_J'(m_J^2).$$

Making in (24) the substitution $M_J \to Z_J^{1/2} M_J$ and introducing the renormalized constant $h_J = Z_J h_{0J}$, we find that (24) is identical to the representation (22) if

$$h_J = Z_J h_{0J} = \frac{h_{0J}}{1 - h_{0J}\tilde{\Pi}_J'(m_J^2)} = \frac{1}{[-\tilde{\Pi}_J'(m_J^2)]}.$$

The last equation is possible as $h_{0J} \to \infty$, i.e., for

$$Z_J = \frac{1}{1 - h_{0J}\tilde{\Pi}_J'(m_J^2)} = 1 + h_J\tilde{\Pi}_J'(m_J^2) = 0, \quad (25)$$

and this is the condition of compositeness of Ref. 24. Thus, the representation (23) with the condition (25) is completely equivalent to (22) and is the basis of our model.

Baryons and other many-quark states can be introduced similarly. These states, described by the method of collective variables, must arise from the terms L_n with $n \geqslant 3$. By means of Fierz transformations, we can separate in L_n a product of colorless n-quark states, which are then identified with the corresponding hadron. Technically, the procedure is the same as when mesons are introduced as two-quark states. However, this program has not yet been realized, since the n-point Green's functions of confined gluons are not known. Therefore, in formulating our model we use an idea that follows from the equivalence of the representations (22) and (23). We shall proceed from the mass spectrum and quantum numbers of the actually existing hadrons and make a natural assumption concerning their quark composition. It is then possible to write down a Lagrangian for the interaction of a hadron with quarks, and the coupling constant is determined from the compositeness condition. Such an approach permits the description of all possible hadronic interactions.

2. MODEL OF CONFINED QUARKS

In this section we shall formulate the model of confined quarks (Quark Confinement Model, QCM), in the framework of which we shall describe the physics of low-energy hadrons. The model is based on the following assumptions.

1. The spectrum of hadrons with masses m_h and quantum numbers J^{CP} is chosen in accordance with the experimental data. It appears to us that in the framework of the assumption (7) the complete spectrum of hadrons cannot be found theoretically, although, in principle, relations between different meson masses can be established.[11] To calculate the complete spectrum, it is necessary to know the gluon Green's function (11) and solve equations of Bethe–Salpeter type.

2. The quark composition of the hadrons is postulated. The Lagrangian of the interaction of the hadrons with the quarks is constructed on the basis of the principle that in the nonrelativistic limit the quarks that form a hadron must be in the state with the lowest orbital angular momentum. This assumption follows directly from (7) and, to all appearances, is valid only for the lowest nonets of hadrons (with masses not greater than 1 GeV). The assumption (7) is not sufficient for the description of hadrons with higher spins and radial excitations, or for many-quark states.

3. The interaction between the hadrons is described by a generating functional of the form (23), in which the hadron–quark coupling constants are determined from the compositeness condition (25).

4. The action of the measure $d\sigma_{\text{vac}}$, which realizes the averaging over the QCD vacuum, ensures confinement of the quarks and convergence of all quark loops.

We consider successively the assumptions of the model.

Suppose that there is a set of hadronic fields H with masses m_h and quantum numbers J^{PC}. We consider successively the mesons, baryons, and many-quark states.

Mesons (two-quark states)

We construct colorless two-quark currents with meson quantum numbers

$$J_J(x) = \bar{q}(x)\,\Gamma_J\, q(x), \quad (26)$$

where the matrix Γ_J ensures the necessary quantum numbers. In general, there may be several such matrices. In particular, the current $\bar{q}(x)\Gamma_J(\overleftrightarrow{\partial}_x\overleftrightarrow{\partial}_x)q(x)$ has the same quantum numbers as (26). We write the coupling of the meson field M_J, which has mass m_J, to the quark currents in the form

$$\mathcal{L}_J = g_J M_J(x) \sum_i c_i J_J^i(x). \tag{27}$$

The sum in (27) is over all two-quark currents that have the necessary quantum numbers. The coefficients c_i satisfy the condition $\Sigma_i c_i^2 = 1$ and are otherwise arbitrary. To construct the Lagrangian (27), we shall proceed from the principle that only currents with the lowest derivatives contribute to $\mathcal{L}_J$. This means that mesons consist of quarks having the lowest orbital angular momentum. Such a state is unique for the majority of the mesons in which we are interested.

Baryons (three-quark states)

The three-quark currents that have the baryon quantum numbers J^P have the form

$$J_B(x) = R_B q^a(x) q^b(x) q^c(x) \varepsilon^{abc}, \tag{28}$$

where R_B is a product of γ matrices, derivatives, and flavor matrices λ_f that act on the quark fields and determine the necessary baryon quantum numbers. The coupling of the baryonic field B, which has mass m_B, to the quark fields is described by the Lagrangian

$$\mathcal{L}_B(x) = g_B \bar{B}_B \sum_i c_i R_B^i q^a q^b q^c \varepsilon^{abc} + \text{h.c.}, \tag{29}$$

where g_B is the coupling constant, and the sum is taken over all possible three-quark currents (29) that have the necessary quantum numbers. As in the case of mesons, the explicit form of the Lagrangian (29) must be determined by the three-point gluon Green's function $G^{a_1a_2a_3}_{\mu_1\mu_2\mu_3}(x_1x_2x_3|B_{\text{vac}})$ (6). Since we do not know this function, we shall, as in the case of mesons, proceed from the principle of the lowest order of the derivatives in the Lagrangian (29).

Many-quark states are constructed similarly. The main difficulty here is that there are many ways in which many-quark states with the necessary quantum numbers can be formed. Therefore, we shall not give here any specific expressions.

The interaction between the hadrons is described by a generating functional completely analogous to (23).

For the calculations, we shall in what follows use the S matrix

$$S = \int d\sigma_{\text{vac}} T \exp\left\{ i \int dx \left[\sum_J \mathcal{L}_J(x) + \sum_B \mathcal{L}_B(x) \right] \right\}. \tag{30}$$

Here, the time ordering is understood as the ordinary Wick time ordering for the hadronic and quark fields, and the propagator of the quark field has the form

$$\overbrace{q_f(x)\bar{q}_{f'}(x')} = \delta_{ff'}(i\hat{\partial}_x + \hat{B}_{\text{vac}}(x))^{-1}\delta(x-x') \tag{31}$$

and after the transition in (30) to normal ordering the quark fields must be set equal to zero. The measure $d\sigma_{\text{vac}}$ acts in exactly the same way as in (22). In what follows we shall use this representation for the S matrix (30).

We turn to the discussion of the *confinement hypothesis*. This hypothesis concerns the definition of the action $d\sigma_{\text{vac}}$ of the gluon vacuum field B_{vac} on the quark fields. This action determines both the mechanism of quark confinement and the dynamics of hadronic interactions at low energies, but at the present time we know least of all about it from the point of view of exact results of theory. Our confinement hypothesis is that quarks in the confinement region do not have a definite value of the mass but are transformed into certain quasiparticles that carry quark quantum numbers but do not exist as ordinary particles. Our ansatz is that in the functional integral (22) the integration of the quark loops over $d\sigma_{\text{vac}}$ can be replaced by the simple integral

$$\int d\sigma_{\text{vac}} \text{tr}\,[M(x_1) S(x_1, x_2 | B_{\text{vac}}) \ldots M(x_n) S \times (x_n, x_1 | B_{\text{vac}})]$$

$$\to \int d\sigma_v \,\text{tr}\,[M(x_1) S_v(x_1 - x_2) \ldots M(x_n) S_v(x_n - x_1)], \tag{32}$$

where

$$S_v(x_1 - x_2) = \int \frac{d^4p}{(2\pi)^4 i} \frac{e^{-ip(x_1-x_2)}}{\Lambda_f v - \hat{p}}. \tag{33}$$

The variable v is dimensionless and varies in the range $-\infty < v < \infty$. The parameter Λ_f, which has the dimensions of mass, depends on the quark flavor and characterizes the size of the region of confinement of the quarks with flavor f. One can also say that Λ_f has the significance of the effective mass of the constituent quark q_f.

Thus, what the confinement ansatz (32) means is that we go over from the functional integral over the vacuum gluon fields in (19) or (24) to the single-parameter integral (32), which effectively takes into account the action of the gluon vacuum on the quark fields.

In the subsequent determination of the measure $d\sigma_v$, we wish to solve two problems: first, to ensure quark confinement, i.e., to guarantee the absence of singularities in the elements of the S matrix associated with the production of quark pairs; second, to achieve ultraviolet convergence of all the integrals that determine all elements of the S matrix. This will enable us to limit the number of independent parameters that occur in the model. The determination of the action of the measure $d\sigma_v$ consists of two parts: the determination of the algebraic nature of the action of the measure in the color space and the determination of its analytic structure.

Algebraic structure of the measure

After the transition to normal ordering in (30), the S matrix is, with respect to the quark variables, a collection of closed colorless quark cycles for mesons, and of more complicated structures in the case of baryons and many-quark states, to which the hadronic fields of the mesons and baryons are joined. Our first assumption is that all these colorless cycles are averaged over the measure $d\sigma_v$ independently, as we discussed in the derivation of (19) from (18), and

$$d\sigma_v = \prod_{a=1}^{3} d\sigma_v^a, \quad \int d\sigma_v^a = 1.$$

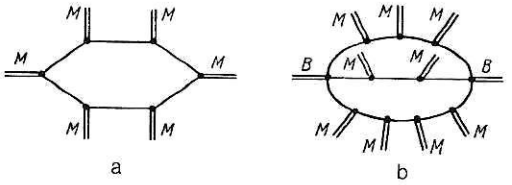

FIG. 1. Quark loop that describes the meson–meson interaction (a) and quark diagram that describes the meson–baryon interaction (b).

The action of the measure $d\sigma_v$ in the quark loops that arise only in the meson–meson interactions (Fig. 1a) is written as

$$\int d\sigma_{\text{vac}} \operatorname{tr}[M(x_1) I^{a_1 a_2} S(x_1, x_2 \mid B_{\text{vac}}) \ldots M(x_n) I^{a_n a_1} S(x_n, x_1 \mid B_{\text{vac}})] \to \to 3 \int d\sigma_v \operatorname{tr}[M(x_1) S_v(x_1 - x_2) \ldots M(x_n) S_v(x_n - x_1)]. \tag{34}$$

We define the amplitudes with the participation of a baryon and mesons (Fig. 1b) as

$$\int d\sigma_{\text{vac}} \varepsilon^{abc} I^{aa'} S^{(k_1)}(x_1, x_2 \mid B_{\text{vac}}) I^{bb'} S^{(k_2)}(x_1, x_2 \mid B_{\text{vac}}) \times I^{cc'} S^{(k_3)}(x_1, x_2 \mid B_{\text{vac}}) \varepsilon^{a'b'c'} \mapsto 6 \prod_{j=1}^{3} S^{(k_j)}(x_1, x_2), \tag{35}$$

where

$$S^{(k)}(x_1, x_2) = \int dy_1 \ldots \int dy_k \int d\sigma_v S_v(x_1 - y_1) M(y_1) \times S_v(y_1 - y_2) \ldots M(y_k) S_v(y_k - x_2). \tag{36}$$

In the diagrams for more complicated processes with the participation of baryons and many-quark states we shall follow the rule that every line with given color is associated with the function (36).

Analytic structure of the measure

The confinement ansatz consists in the determination of the analytic structure of the measure $d\sigma_v$, i.e., in the definition of the integral

$$\int \frac{d\sigma_v}{v - z} = G(z) = a(-z^2) + zb(-z^2). \tag{37}$$

We shall call the function $G(z)$ the confinement function. It is assumed that $G(z)$ satisfies the following conditions:

1. $G(z)$ is universal, i.e., it does not depend on the color and flavor [at least for the flavor group SU(3)]. In other words, the function $G(z)$ is the same for all quark structures determining the interaction of mesons, baryons, and other many-quark hadrons.

2. $G(z)$ is an entire function, analytic in the plane of the complex variable z. This condition ensures quark confinement and unitarity of the S matrix in the hadronic sector of the state space.

3. $G(z)$ decreases faster than any polynomial in the Euclidean domain, i.e.,

$$\lim_{z^2 \to -\infty} (-z^2)^N \mid G(z) \mid = 0$$

for any $N > 0$. This condition ensures convergence of all quark diagrams.

4. The explicit form of the function $G(z)$ cannot yet be found from any general arguments. Therefore, the choice of the confinement function also belongs to the ansatz of the model. However, as calculations showed, for satisfactory description of low-energy processes with the participation of mesons and baryons it is the integrated properties of the function $G(z)$ that are basically important. The series of calculations made in the study of Ref. 25 used the function

$$G(z) = \exp(a + bz + z^2). \tag{38}$$

Below, we shall discuss other possible choices of the function $G(z)$.

5. In the calculation of the elements of the S matrix, all the calculations must be made in the Euclidean metric, with a subsequent transition to the physical domain of the momentum variables by analytic continuation of the elements of the S matrix with respect to the invariant momentum variables.

The functions corresponding to the quark loops calculated in accordance with the rule (32) with a confinement function $G(z)$ that satisfies the conditions listed above are entire analytic functions in the external momentum variables. In other words, the quark loops do not contain singularities associated with the production of quark pairs. The S matrix (30), constructed in accordance with all the rules listed above, belongs to the class of theories with nonlocal interaction investigated in the book of Ref. 26. It is unitary and macrocausal in the hadronic sector in each order of the expansion in powers of the interaction Lagrangian.

Thus, the compositeness condition and the confinement ansatz have the consequence that in a system of hadrons and quarks described by Lagrangians of the form (27) and (29) only the hadronic degrees of freedom are physically observable, and the quarks appear as auxiliary virtual particles that determine the hadronic interactions and thereby describe the internal structure of the hadrons. From the point of view of quark–hadron duality, we are in the hadronic sector, and the quarks that occur in the Lagrangians (27) and (29) have the meaning of constituent virtual particles that are absent as observable objects in the space of the physical states.

3. AMPLITUDES OF PHYSICAL PROCESSES IN THE QCM

The representation (30) gives the S matrix which describes all possible hadron-interaction processes. When the S matrix is expanded in powers of the interaction Lagrangians, matrix elements representing quark loops coupled by hadronic lines arise.

The hadron–quark coupling constants must be calculated from the compositeness condition (25), which, in essence, is a condition of strong coupling. Thus, our theory describes strong interactions, and therefore perturbation theory in the coupling constant is not valid in calculations. How shall we make the calculations? We first recall that the derivation of the compositeness condition[24] presupposes the validity of successive subsummations of classes of diagrams of chain type for the hadron Green's functions and of the matrix elements of hadronic processes in a perturbation-theory series. Therefore, our calculations will also be based on approximations associated with the summation of definite

classes of diagrams for the hadron Green's functions. We shall make these approximations in the framework of the so-called $1/N_c$ expansion. In the representation of the S matrix as a sum of Feynman diagrams, the quarks appear only in the form of closed loops. It follows from the compositeness condition (25) that the effective strong coupling constant is

$$h_J = 4N_c g_J^2/(4\pi)^2 = 3g_J^2/(2\pi)^2, \tag{39}$$

where $N_c = 3$ is the number of colors.

Therefore, the perturbation series can be represented as an expansion in two parameters: h_J and

$$\varepsilon_c = 1/N_c = 1/3. \tag{40}$$

Our approximations will be associated with the expansion with respect to the parameter ε_c. Thus, we shall estimate the theoretical error of the model at around 20–30%.

We shall consider in detail the first two approximations.

First approximation

We shall call this the single-loop approximation. We consider the Green's function of a hadron (to be definite, we shall speak only of scalar or pseudoscalar mesons). In the zeroth approximation in ε_c the Green's function is determined solely by single-loop quark diagrams of chain form, shown in Fig. 2a, and can be expressed with allowance for mass renormalization in the form

$$D(p^2) = \frac{1}{m^2 - p^2 + h_0[\tilde{\Pi}(p^2) - \tilde{\Pi}(m^2)]} \xrightarrow[p^2 \to m^2]{} \frac{Z}{m^2 - p^2}, \tag{41}$$

$$Z = \frac{1}{1 - h_0 \tilde{\Pi}'(m^2)}.$$

The meson mass operator $\tilde{\Pi}(p^2)$ in (41) corresponds to a single-loop quark diagram. The renormalized coupling constant is determined by the relation

$$h = Zh_0,$$

whence

$$Z = 1 + h\tilde{\Pi}'(m^2)$$

and from the compositeness condition (25) we have

$$h = 1/[-\tilde{\Pi}'(m^2)]. \tag{42}$$

For the Green's function we obtain

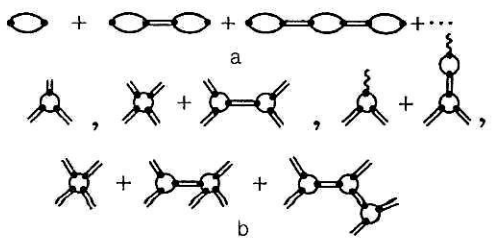

FIG. 2. First (single-loop) approximation in $1/N_c$: a) Green's function; b) amplitudes of physical processes.

$$h_0 D(p^2) = \frac{Zh_0}{Z(m^2 - p^2) + Zh_0[\tilde{\Pi}(m^2) - \tilde{\Pi}(p^2)]} = hD_r(p^2),$$

$$D_r(p^2) = \frac{\tilde{\Pi}'(m^2)}{\tilde{\Pi}(m^2) - \tilde{\Pi}(p^2)}. \tag{43}$$

We shall say a few words about the analytic structure of the Green's function (43). The mass operator $\tilde{\Pi}(p^2)$ is an entire analytic function in the p^2 plane and does not contain any threshold singularities. The Green's function of the single-loop approximation has on the real axis of p^2 only a single pole at $p^2 = m^2$, which determines the mass of the meson. In the complex p^2 plane, the function $D_r(p^2)$ has poles corresponding to the complex zeros of the function $\tilde{\Pi}(m^2) - \tilde{\Pi}(p^2)$. These poles are unphysical and are due to the expansion in ε_c that we are using. It is important that as $p^2 \to -\infty$, the function behaves as $D_r(p^2) \to O(1)$. Thus, the single-loop approximation correctly reproduces the behavior of the hadron Green's functions only near the mass shell of the hadrons, i.e., in the infrared limit at low energies.

We note further that the first approximation corresponds in the representation (24) to unification of the free Lagrangian of the meson with the mass operator in the single-loop approximation:

$$D_r^{-1}(p^2) = m^2 - p^2 + h\tilde{\Pi}_{\text{reg}}(p^2)$$
$$= m^2 - p^2 - \frac{1}{\tilde{\Pi}'(m^2)}[\tilde{\Pi}(p^2) - \tilde{\Pi}'(m^2) - \tilde{\Pi}'(m^2)(p^2 - m^2)]$$
$$= \frac{\tilde{\Pi}(m^2) - \tilde{\Pi}(p^2)}{\tilde{\Pi}'(m^2)}.$$

In the single-loop approximation, the amplitudes of the hadronic processes are described by single-loop quark diagrams, which are tree diagrams with respect to the hadronic lines. Examples of such diagrams are shown in Fig. 2b. With each internal hadronic line there is associated the propagator of the hadron of the single-loop approximation (43).

The quark loops shown in Fig. 2b are entire analytic functions in the external momenta of the hadrons and, therefore, do not have any threshold singularities. On the one hand, this corresponds to complete quark confinement; on the other, it shows that the single-loop approximation is valid for not too high hadron energies, i.e., as long as the influence of the possible intermediate processes can be ignored.

Thus, the single-loop approximation completely corresponds to the tree diagrams of chiral theory. However, an important difference is that in the chiral theory the hadron–hadron vertices are structureless points, i.e., they correspond to a local interaction of hadrons, whereas in our model the hadron–hadron vertices are described by quark loops, which determine the structure of the hadrons—form factors, slope parameters, etc.

Second approximation

The corrections linear in $\varepsilon_c = 1/N_c$ to the hadron mass operator are determined by the diagrams shown in Figs. 3a and 3b, in which the internal meson lines are associated with the propagator (43) of the single-loop approximation:

$$h\tilde{\Pi}^{(2)}(p^2) = h\int dk\Gamma_{(a)}(p, k)\frac{1}{\tilde{\Pi}(m^2) - \tilde{\Pi}(k^2)}$$
$$+ h\int\int dk_1\, dk_2\, \Gamma_b(k_1, k_2, p)\prod_{j=1}^{2}\frac{1}{\tilde{\Pi}(m^2) - \tilde{\Pi}(k_j^2)}\delta$$
$$\times(p - k_1 - k_2). \tag{44}$$

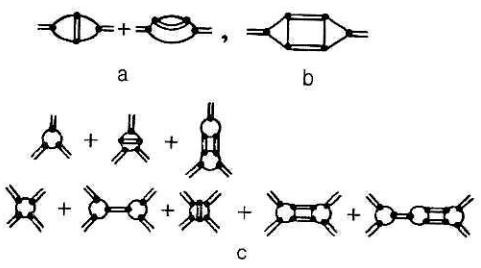

FIG. 3. Second approximation in $1/N_c$: a), b) Green's function; c) amplitudes of physical processes.

Here, the first term corresponds to the diagrams in Fig. 3a, and the second to those in Fig. 3b. The functions $\Gamma_{(a)}(p,k)$ and $\Gamma_{(b)}(k_1, k_2, p)$, which determine the quark loops, decrease in the Euclidean domain as $O[1/(-k^2)]$ when $k^2 \to -\infty$, while the hadron propagators (43) of the single-loop approximation tend to constants. Therefore, the integrals in (44) diverge quadratically.

We renormalize the hadron Green's functions in such a way that the hadron mass and the coupling constant are determined by the equations of the single-loop approximation. We obtain

$$D_2(p^2) = \frac{\widetilde{\Pi}'(m^2)}{\widetilde{\Pi}(m^2) - \widetilde{\Pi}(p^2) - \dfrac{\varepsilon_c}{\widetilde{\Pi}'(m^2)}\widetilde{\Pi}^{(2)}_{\text{reg}}(p^2)}, \tag{45}$$

where

$$\widetilde{\Pi}^{(2)}_{\text{reg}}(p^2) = \widetilde{\Pi}^{(2)}(p^2) - \widetilde{\Pi}^{(2)}(m^2) - \widetilde{\Pi}^{(2)\prime}(m^2)(p^2 - m^2).$$

As $p^2 \to m^2$,

$$D_2(p^2) \to \frac{1}{m^2 - p^2}.$$

As $p^2 \to -\infty$,

$$D_2(p^2) \to \frac{\text{const}}{(-p^2)\ln(-p^2)}.$$

The Green's function (45) of the second approximation has on the real axis of p^2 a pole at the point $p^2 = m^2$ and two-particle threshold singularities corresponding to intermediate two-meson states. In addition, there are unphysical singularities associated with the use of the expansion in ε_c.

In this approximation, the amplitudes of the hadronic processes are described by diagrams of which examples are given in Fig. 3c, in which the internal meson lines are associated with the propagator (45). These amplitudes have two-particle threshold singularities with respect to the external momenta of the hadrons. This approximation is valid at higher energies than the single-loop approximation.

The diagrams of the second approximation of the form shown in Fig. 4b diverge logarithmically. The divergence can be eliminated by a renormalization of the coupling constant in the diagram shown in Fig. 4a. Thus, we have

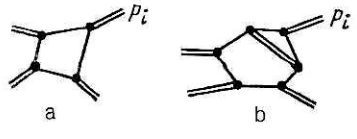

FIG. 4. Renormalization of coupling constants in the second approximation in $1/N_c$.

$$T^{(2)}(p_i^2, \ldots) \to T^{(2)}_{\text{reg}}(p_i^2, \ldots) = T^{(2)}(p_i^2, \ldots) - T^{(2)}(m^2, \ldots).$$

The rules which we have formulated completely determine the second approximation of the $1/N_c$ expansion in our model.

The following expansions in the parameter $\varepsilon_c = 1/N_c$ can be constructed similarly.

4. THE QCM AND LOW-ENERGY RELATIONS

In the QCM, the hadronic interactions are determined by the quark structure of the hadrons and the quark behavior at large distances. It is important that the model permits calculation of not only the static properties (lifetimes, magnetic moments, electromagnetic radii, etc.) but also the momentum dependence of physical matrix elements (slope parameters, form factors, etc.).

In this paper, we shall consider only low-energy meson physics. For application of the methods of the QCM to nucleon physics, see Ref. 27.

We write the meson–quark interaction Lagrangian in the form

$$\mathcal{L}_I = \frac{g_M}{\sqrt{2}} \sum_{i=1}^{8} M_i \bar{q} \Gamma_M \lambda_i q. \tag{46}$$

Here, M_i are Euclidean fields related to the physical fields of the mesons in the standard manner[28]; λ_i are Gell-Mann matrices ($\lambda_0 = \sqrt{2/3}I$); Γ_M are the corresponding Dirac matrices; $i\gamma^5$ is for pseudoscalar mesons $P(\pi, K, \eta, \eta')$; γ^μ is for vector mesons $V(\pi, K^*, \omega, \varphi)$; $\gamma^\mu\gamma^5$ is for axial mesons $A(a_1, k_1, f_1)$; and $I - i\overleftrightarrow{\hat{\partial}}/\Lambda$ is for scalar mesons $S(a_0, k_0, f_0, \varepsilon)$. The role of the additional term with the derivative in the case of scalar mesons will be discussed in detail in Sec. 6.

The mixing angles for the octet and the singlet state are defined as follows:

$$\left.\begin{aligned} &(\eta', \omega, \varepsilon) \to \cos\delta \frac{\bar{u}u + \bar{d}d}{\sqrt{2}} - \bar{s}s \sin\delta; \\ &(\eta, \varphi, f_0) \to -\sin\delta \frac{\bar{u}u + \bar{d}d}{\sqrt{2}} - \bar{s}s \cos\delta, \quad \delta = \theta - \theta_I. \end{aligned}\right\} \tag{47}$$

The coupling constants g_M are determined from the compositeness condition (25). It is convenient to introduce the effective coupling constants

$$h_M = 3g_M^2/(2\pi)^2.$$

We first discuss the choice of the basic parameters of the model and obtain the connection between its predictions and the well-known low-energy relations.[29] The basic phenomenological quantities in the QCM are the confinement functions $a(u)$ and $b(u)$ (37) and the dimensional parameters Λ_f, which characterize the confinement region of the quarks with flavor $f(\Lambda \equiv \Lambda_u = \Lambda_d, \Lambda_s)$. The functions $a(u)$ and $b(u)$ must satisfy the requirements listed above, and their form must be analogous to that of the functions shown in Fig. 5. For the actual calculations, we choose $a(u)$ and $b(u)$ in the simplest form:

$$\begin{aligned} a(u) &= a_0 \exp[(-u^2 - 2a_1 u); \\ b(u) &= b_0 \exp(-u^2 + 2b_1 u). \end{aligned} \tag{48}$$

We determine the parameters a_0, b_0, a_1, b_1, Λ, and Λ_s by a fit to well-established experimental quantities, which are the

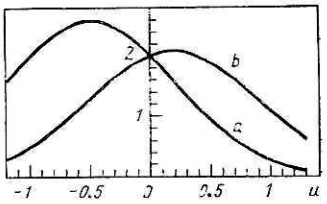

FIG. 5. Confinement functions $a(u) = 2\exp(-u^2-u)$, $b(u) = 2\exp(-u^2+0.4u)$.

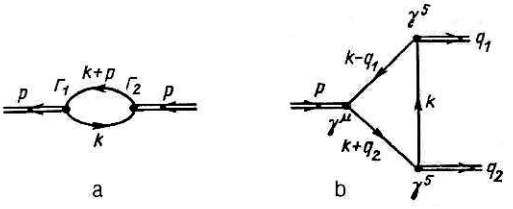

FIG. 6. Two-vertex (a) and three-vertex (b) quark loops.

input parameters of the main widely accepted phenomenological approaches.

We make some remarks concerning descriptions of the well-known low-energy relations[29] in the framework of the QCM.

It is important that the procedure for integration with respect to $d\sigma_v$ defined by Eq. (37) preserves gauge invariance at all stages of the calculations. For example, the expression for the two-point diagram that describes the vector–vector transition (Fig. 6a) has the manifestly gauge-invariant form

$$\int \frac{d^4k}{4\pi^2 i} \int d\sigma_v \,\mathrm{tr}\left[\gamma^\mu \frac{1}{v\Lambda - \hat{k}} \gamma^\nu \frac{1}{v\Lambda - \hat{k} - \hat{p}}\right] = [p^\mu p^\nu - p^2 g^{\mu\nu}]\,\frac{1}{3} R_V(w), \tag{49}$$

where $w = p^2/\Lambda^2$ and

$$R_V(w) = B_0 + \frac{w}{4}\int_0^1 dub\left(-u\frac{w}{4}\right)\sqrt{1-u}\left(1+\frac{u}{2}\right).$$

The expression (49) is finite and does not contain an imaginary part corresponding to quark production.

For the quark diagram describing the axial–axial transition ($\Gamma_1 = \mu^\mu\gamma^5$; $\Gamma_2 = \gamma^\nu\gamma^5$; see Fig. 6a), we have the expression

$$\int \frac{d^4k}{4\pi^2 i} \int d\sigma_v \,\mathrm{tr}\left[\gamma^\mu\gamma^5 \frac{1}{v\Lambda - \hat{k}} \gamma^\nu\gamma^5 \frac{1}{v\Lambda - \hat{k} - \hat{p}}\right] = [p^\mu p^\nu - p^2 g^{\mu\nu}]\,\frac{1}{3} R_V(w) + g^{\mu\nu}\frac{2\Lambda^2}{3} R_A(w). \tag{50}$$

The explicit form of the function $R_A(w)$ is given in Table I. As one would expect from the ansatz (37), chiral invariance is broken, and the measure of its breaking is the parameter Λ.

Further, we consider how the anomalous Ward identities are obtained in our approach. To this end, we calculate triangle diagrams: 1) $\Gamma_1 = \gamma^5$, $\Gamma_2 = \gamma^\mu$, $\Gamma_3 = \gamma^\nu$; 2) $\Gamma_1 = \gamma^\alpha\gamma^5$, $\Gamma_2 = \gamma^\mu$, $\Gamma_3 = \gamma^\nu$ (see Fig. 6b) in the limit of small pion momenta.

We have

TABLE I. Structure integrals.

$R_{PP}(w) = B_0 + \frac{w}{4}\int_0^1 dub\left(-u\frac{w}{4}\right)\frac{(1-u/2)}{\sqrt{1-u}}$
$R_{VV}(w) = B_0 + \frac{w}{4}\int_0^1 dub\left(-u\frac{w}{4}\right)\frac{(1-u/2+u^2/4)}{\sqrt{1-u}}$
$R_V(w) = B_0 + \frac{w}{4}\int_0^1 dub\left(-u\frac{w}{4}\right)\sqrt{1-u}\left(1+\frac{u}{2}\right)$
$R_P(w) = A_0 + \frac{w}{4}\int_0^1 dua\left(-u\frac{w}{4}\right)\sqrt{1-u}$
$R_{PVV}(w) = \frac{1}{4}\int_0^1 dua\left(-u\frac{w}{4}\right)\ln\left(\frac{1+\sqrt{1-u}}{1-\sqrt{1-u}}\right)$
$R_{VPP}(w) = B_0 + \frac{w}{4}\int_0^1 dub\left(-u\frac{w}{4}\right)\sqrt{1-u}$
$R_A(w) = B_1 - \left(\frac{w}{4}\right)^2\int_0^1 duub\left(-u\frac{w}{4}\right)\sqrt{1-u}$
$A_0 = \int_0^\infty dua(u) = 1.09; \quad B_0 = \int_0^\infty dub(u) = 2.26;$ $B_1 = \int_0^\infty duub(u) = 1.45$

$$T_5^{\mu\nu} = \int \frac{d^4k}{4\pi^2 i} \int d\sigma_v \operatorname{tr} [\gamma^5 S_v(\hat{k}) \gamma^\mu S_v(\hat{k}+\hat{q}_1) \gamma^\nu S_v(\hat{k}+\hat{p})]$$

$$= i\varepsilon^{\mu\nu\alpha_1\alpha_2} q_1^{\alpha_1} q_2^{\alpha_2} \frac{1}{4\Lambda} \int_0^1 du a\left(-u\frac{w}{4}\right) \ln\left[\frac{1+\sqrt{1-u}}{1-\sqrt{1-u}}\right]$$

$$\simeq i\varepsilon^{\mu\nu\alpha_1\alpha_2} q_1^{\alpha_1} q_2^{\alpha_2} \frac{1}{2\Lambda}\left[a(0) + w\left(-\frac{a'(0)}{12}\right)\right]. \quad (51)$$

To obtain the anomalous identities, we calculate the convolution

$$p^\alpha T_5^{\alpha\mu\nu} = \int \frac{d^4k}{4\pi^2 i} \int d\sigma_v \operatorname{tr}$$

$$\times [\hat{p}\gamma^5 S_v(\hat{k}) \gamma^\mu S_v(\hat{k}+\hat{q}_1) \gamma^\nu S_v(\hat{k}+\hat{p})]$$

$$= i\varepsilon^{\mu\nu\alpha_1\alpha_2} q_1^{\alpha_1} q_2^{\alpha_2} \frac{w}{8} \int_0^1 du u b\left(-u\frac{w}{4}\right) \ln\left[\frac{1+\sqrt{1-u}}{1-\sqrt{1-u}}\right]$$

$$= i\varepsilon^{\mu\nu\alpha_1\alpha_2} q_1^{\alpha_1} q_2^{\alpha_2} w [b(0)/12]. \quad (52)$$

Comparing (51) and (52), we obtain

$$p^\alpha T_5^{\alpha\mu\nu} = 2\Lambda\left[-\frac{b(0)}{a'(0)}\right] T_5^{\mu\nu}$$

$$- 2i\varepsilon^{\mu\nu\alpha_1\alpha_2} q_1^{\alpha_1} q_2^{\alpha_2}\left[-\frac{b(0)\, a(0)}{a'(0)\, 2}\right]. \quad (53)$$

If the identity (53) is to be completely identical to the usual anomalous Ward identity,[30] it is sufficient to require the following conditions on the behavior of the functions $a(u)$ and $b(u)$ at the origin:

$$b(0) = -a'(0), \quad a(0) = 2.$$

Hence

$$a_0 = 2, \quad b_0 = -4a_1. \quad (54)$$

Condition (54) leaves only two coefficients b_0 and b_1 free; these characterize the form of the function $b(u)$.

We fix the parameters b_0, b_1, and Λ by a fit to the following quantities: first, the pion weak-decay constant $f_\pi = 132$ MeV, which is a fundamental constant in chiral theories[29]; second, the constant of the transition $\rho \to \gamma$, which determines the vector-dominance model; third, the constants that determine the decays $\pi^0 \to \gamma\gamma$ and $\omega \to \pi\gamma$. These constants are usually determined by the Adler anomalies.[29] Finally, we have the strong-decay constant for $\rho \to \pi\pi$, which in the vector-dominance model is directly related to the constant of the transition $\rho \to \gamma$.

It was found that the best description of the experimental data is achieved in the case

$$a_0 = b_0 = 2; \quad a_1 = 0.5; \quad b_1 = 0.2; \quad \Lambda = 460 \text{ MeV}. \quad (55)$$

The results of the fit are given in Table II. The structure integrals that determine the physical quantities are given in Table I. We have used the notation $w_M = m_M^2/\Lambda^2$. It can be seen that there is good agreement with the experimental data.

We also give expressions for the physical quantities in the case of vanishing meson masses. It is readily seen that in this case the QCM reproduces with an error of 4–5% the well-known low-energy relations: the Goldberger–Treiman relation, the hypothesis of ρ universality, and the relations between $g_{\pi\gamma\gamma}$ and f_π, $g_{\pi\gamma\gamma}$, and $g_{\omega\pi\gamma}$ obtained from the anomalous identities and PCAC.[29]

We fix the parameter Λ_s which characterizes the confinement region of the strange quark, by a fit to the main decays of the strange mesons: $K \to \mu\nu$, $K^* \to K\pi$, $K^* \to K\gamma$, $\varphi \to K^+K^-$, $\varphi \to e^+e^-$. The best agreement with the experimental data is obtained for

TABLE II. Main low-energy quantities in the QCM.

Process	Observed quantity	Value of constant for $m = 0$	Experiment[38]
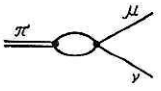	$f_\pi = \frac{\Lambda}{\pi}\frac{\sqrt{3}R_P(w_\pi)}{\sqrt{2R_{PP}(w_\pi)}} = 132$ MeV	$f_\pi^{(0)} = 0.96\frac{\Lambda}{g_{\pi\gamma}^{(0)}}$	132 MeV
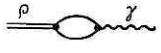	$g_{\rho\gamma} = \frac{R_V(w_\rho)}{\pi\sqrt{8R_{VV}(w_\rho)}} = 0.18$	$g_{\rho\gamma}^{(0)} = 1{,}07/2\pi$	0.20
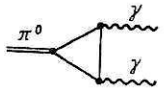	$g_{\pi\gamma\gamma} = \frac{1}{\Lambda}\frac{R_{PVV}(w_\pi)}{\pi\sqrt{3R_{PP}(w_\pi)}} = 0.26$ GeV^{-1}	$g_{\pi\gamma\gamma}^{(0)} = 0.96/(2\sqrt{2}\,\pi^2 f_\pi^{(0)})$	0.276 GeV^{-1}
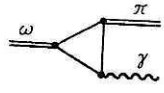	$g_{\omega\pi\gamma} = \frac{1}{\Lambda}\frac{\sqrt{6}R_{PVV}(w_\omega)}{\sqrt{R_{PP}(w_\pi)R_{VV}(w_\omega)}} = 2.10$ GeV^{-1}	$g_{\omega\pi\gamma}^{(0)} = 0.94\cdot 3\,\pi g_{\pi\gamma\gamma}^{(0)}$	2.54 GeV^{-1}
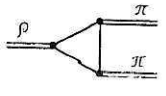	$g_{\rho\pi\pi} = \frac{\pi\sqrt{8}R_{VPP}(w_\rho)}{R_{PP}(w_\pi)\sqrt{R_{VV}(w_\rho)}} = 6.0$	$g_{\rho\pi\pi}^{(0)} = \frac{1}{g_{\rho\gamma}^{(0)}}$	6.1

TABLE III. Main processes with strange quarks.

Process	Observed quantity	QCM	Experiment[38]
$K \to \mu\nu$	f_K	160 MeV	157 MeV
$\varphi \to \gamma$	$g_{\varphi\gamma}$	0.0901	0.0758
$K^* \to K\gamma$	$g_{K^*K\gamma}$	1.17 GeV^{-1}	(1.29±0.07) GeV^{-1}
$K^* \to K\pi$	$g_{K^*K\pi}$	4.22	4.65
$\varphi \to K\bar{K}$	$g_{\varphi K\bar{K}}$	4.04	4.47±0.14

$$\Lambda_s = 506 \text{ MeV}. \tag{56}$$

The results of the fit are given in Table III. It can be seen that there is good agreement with the experiments.

It is interesting to note that the parameters Λ_s and $\Lambda = \Lambda_u = \Lambda_d$ were found to have nearly equal values. This is explained by the fact that in the considered approach the SU(3) symmetry is broken mainly through the difference of the masses of the mesons that contain strange quarks and the masses of the mesons that contain nonstrange quarks; these occur in the structure integrals that determine the matrix elements of the physical processes.

Thus, all the parameters of the model are fixed.

5. FORM FACTORS, RADII, AND SLOPE PARAMETERS

The next step in testing the basic assumptions of the model is to study the momentum dependence of the matrix elements of the physical processes that is due to the quark structure of the hadrons. In this section, we consider successively the slope parameters in the Dalitz decays $P\to\gamma l^+l^-$ ($P=\pi^0,\eta,\eta'$), $V\to Pl^+l^-$ and the widths of the rare decays $P\to l^+l^-$; the behavior of the pion form factor F_π (q^2) both in the Euclidean ($q^2\leqslant 0$) and in the physical ($q^2\geqslant 0$) domain; the ratio of the axial and vector form factors $\gamma = f_A/f_V$ in the electroweak decay $\pi^-\to ev\gamma$; the electromagnetic radii of kaons; and the parameters of K_{l_3} decay.

The Dalitz decays $P\to\gamma l^+l^-$ and $V\to Pl^+l^-$ and the rare decays $P\to l^+l^-$

The investigation of the electromagnetic structure of the neutral particles ($P=\pi^0,\ \eta,\ \eta',\ V=\rho^0,\ \omega,\ \varphi$) involves

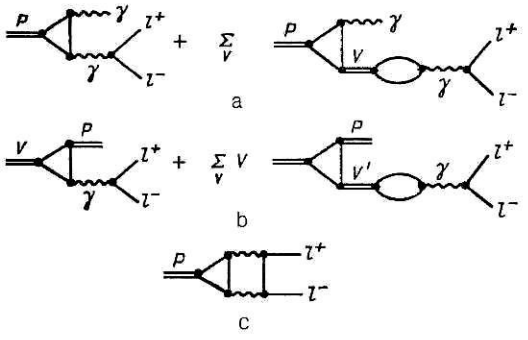

FIG. 7. Quark diagrams that describe Dalitz decays: a) of pseudoscalar mesons, $P\to\gamma l^+l^-$; b) of vector mesons, $V\to Pl^+l^-$; c) rare decays $P\to l^+l^-$

study of processes with the participation of two photons, $P\to\gamma\gamma, P\to\gamma l^+l^-, P\to l^+l^-$, or of processes with a change of the C parity of the hadrons in the initial and final states: $V\to Pl^+l^-$ and $P\to Vl^+l^-$.

We consider decays of neutral pseudoscalar mesons, $P\to\gamma l^+l^-$ (Fig. 7a). This decay is described by an anomalous triangle diagram and a resonance diagram with intermediate vector mesons ($\rho,\ \omega,\ \varphi$). The corresponding structure form factor can be represented in the form

$$G_{P\gamma\gamma}(p^2,\ q_1^2,\ q_2^2) = g_{P\gamma\gamma}(p^2,\ q_1^2,\ q_2^2) + \sum_V g_{VP\gamma}(p^2, q_1^2,\ q_2^2)\, g_{V\gamma}(q_2^2)\, D_V(q_2^2)\, q_2^2. \tag{57}$$

The slope parameters in the decay $P\to\gamma l^+l^-$ are defined as[31]

$$\frac{1}{M_P^2} = \frac{G'_{P\gamma\gamma}(m_P^2,\ 0,\ 0)}{G_{P\gamma\gamma}(m_P^2,\ 0,\ 0)}. \tag{58}$$

The slope parameters in the decay $V\to Pl^+l^-$ (see Fig. 7b) are calculated similarly. Numerical results are given in Table IV. For comparison we give the results obtained in the vector-dominance model (VDM).

It can be seen that the contribution from the resonance diagrams is somewhat reduced in comparison with the VDM results. This is due to the allowance for the dependence of the function $g_{V\gamma}(q^2)$ on the momentum of the vector meson. At the same time, for the light mesons (π^0 and η) an important part is played by the contribution from the triangle diagram, so that the total values are close to the VDM predictions. For the heavy mesons ($\eta',\ \omega$), the contribution from the triangle diagram is negligibly small.

Experimental measurements of the slope parameters were made in Ref. 32 for $\pi^0\to\gamma e^+e^-$ and in Refs. 33 and 34 for $\eta,\ \eta'\to\gamma\mu^+\mu^-$ and $\omega\to\pi^0\mu^+\mu^-$. The numerical values are given in Table IV.

We note that in the determination of the slope parameter in the decay $\pi^0\to\gamma e^+e^-$ (Ref. 32) an important part is played by the radiative corrections, allowance for which increases the value of the slope parameter by more than a factor 2.[31] The theoretical values for this parameter, obtained both in the QCM and VDM and in a number of other models,[31] are given without allowance for radiative corrections. In the case of the decays $\eta,\ \eta'\to\gamma\mu^+\mu^-$ and $\omega\to\pi^0\mu^+\mu^-$ the radiative corrections are negligibly small.[31]

It can be seen from Table IV that the value for the slope parameter in the decay $\eta\to\gamma\mu^+\mu^-$ obtained in the QCM is in good agreement with experiment,[31] whereas the values of

TABLE IV. Numerical values for the slope parameters $1/M^2$, in GeV^{-2}.

Process		VDM	Experiment
$\pi^0 \to \gamma e^+e^-$	0.39+1.18 1.57	1.67	5.5±1.6 (Ref. 32)
$\eta \to \gamma\mu^+\mu^-$	0.33+1.81=2.14 (−11°) 0.31+1.64=1.95 (−18°)	2.6 (−11°) 2.4 (−18°)	1.9±0.4 (Ref. 31)
$\eta' \to \rho\mu^+\mu^-$	−0.044+0.82=0.77 (−11°) −0.041+0.73=0.69 (−18°)	1.1 (−11°) 0.95 (−18°)	1.7±0.4 (Ref. 31)
$\omega \to \pi^0\mu^+\mu^-$	0.089+1.21=1.30	1.69	2.4±0.2 (Ref. 31)

the slope parameters in the decays $\eta' \to \gamma\mu^+\mu^-$ and $\omega \to \pi^0\mu^+\mu^-$ are about 2 times less than the existing experimental values.[31] In the case of large meson masses ($m_{\eta'} = 958$ MeV, $m_\omega = 780$ MeV) it is evidently necessary to take into account the heavy vector mesons (ρ',...), and also two-particle intermediate states (2π,...). In addition, a higher accuracy is also required in the experimental measurements.

Experimentally rare decays $P \to l^+l^-$ have been discovered[35,36] in which the lepton pair is coupled to the hadron vertex by two virtual photons. To describe the rare decays $P \to l^+l^-$, it is necessary to know the behavior of the transition form factor $G_{P\gamma\gamma}(p^2, q_1^2, q_2^2)$ both in the spacelike region $q_i^2 \leqslant 0$ and in the timelike pre-threshold region $0 \leqslant q_i^2 \leqslant 4m_P^2$. Using unitarity relations, one can relate the imaginary part of the $P \to l^+l^-$ amplitude to the $P \to \gamma\gamma$ process and, thus, find a lower bound for the width of this decay, which is called the unitarity limit[37]:

$$\frac{\Gamma(P \to l^+l^-)}{\Gamma(P \to \gamma\gamma)} \geqslant 2\alpha^2 \left(\frac{m_l}{m_P}\right)^2 \frac{\left[\ln \frac{1+\sqrt{1-4m_l^2/m_P^2}}{2m_l/m_P}\right]^2}{\sqrt{1-4m_l^2/m_P^2}}.$$

The corresponding values of the unitarity limit for various decay modes are given in Table V. However, the total probability is determined by the contributions of both the imaginary and the real parts of the amplitude.

In the QCM, the decays $P \to l^+l^-$ are determined by the diagram of Fig. 7c, and the corresponding matrix element can be written in the form

$$M(P \to l^+l^-) = e^4\varepsilon^{\mu\rho\sigma\nu} \int \frac{d^4k}{(2\pi)^4 i} p^\rho k^\sigma g_{P\gamma\gamma}(p^2, (p-k)^2, k^2) \times \frac{\bar{v}(p_-)\gamma^\mu(m_l + \hat{k} - \hat{p}_+)\gamma^\nu v(p_+)}{k^2(k-p)^2[m_l^2 - (k-p_+)^2]}, \quad (59)$$

where p is the momentum of the decaying meson, and p_+ and p_- are the momenta of the final leptons. Expanding the integral (59) in a series in the small parameter m_l^2/m_P^2, we obtain

$$M(P \to l^+l^-) = \alpha^2 g_{P\gamma\gamma}\varepsilon^{\mu\rho\nu\sigma} p^\rho \bar{v}(p_-)\gamma^\mu\gamma^\alpha\gamma^\nu v(p_+) \times \left[\frac{1}{4} g^{\sigma\alpha} I - (P_+^\sigma P_+^\alpha / p^2) N\right], \quad (60)$$

where

$$g_{P\gamma\gamma} = g_{P\gamma\gamma}(m_P^2, 0, 0);$$

$$I = \ln \frac{m_P^2}{\Lambda^2} - 7/2 - r - i\pi;$$

$$r = \int_0^\infty dt \ln t\,[t(t+1) - 1/2]\, a(t) = 0.018;$$

$$N = \left[2\ln^2 \frac{m_l^2}{m_P^2} + 6\ln \frac{m_l}{m_P} + 3\right] - i\pi\left[2\ln \frac{m_l}{m_P} + 3\right].$$

Calculating the $P \to l^+l^-$ decay width in the standard manner, we finally obtain

$$\frac{\Gamma(P \to l^+l^-)}{\Gamma(P \to \gamma\gamma)} = \frac{1}{2}\left(\frac{\alpha m_l}{\pi m_P}\right)^2 \beta\{9|I|^2 + \beta^4|N|^2 + 6\beta^2[\text{Re } I \text{ Re } N - \text{Im } I \text{ Im } N]\}, \quad (61)$$

$$\beta = \sqrt{1-4m_l^2/m_P^2}.$$

The results of the calculations are given in Table V. The predictions of the QCM are close to the mean experimental value in the decay $\eta \to \mu^+\mu^-$, although the experimental errors are still large. The experimental value of the relative probability of the $\pi^0 \to e^+e^-$ decay has large statistical errors, which are given at the 90% confidence level. The values for the remaining quantities are predictions of the model,

TABLE V. Value of the ratio $\Gamma(P \to l^+l^-)/\Gamma(P \to \gamma\gamma)$.

Process	Experiment[35,36]	Unitarity limit[37]	QCM
$\pi^0 \to e^+e^-$	$22^{+27}_{-11}\cdot 10^{-8}$	$4.6\cdot 10^{-8}$	$5.4\cdot 10^{-8}$
$\eta \to \mu^+\mu^-$	$(1.7\pm 0.5)\cdot 10^{-5}$	$1.2\cdot 10^{-5}$	$2.4\cdot 10^{-5}$
$\eta \to e^+e^-$	—	$4.3\cdot 10^{-9}$	$9.9\cdot 10^{-9}$
$\eta' \to \mu^+\mu^-$	—	$4.1\cdot 10^{-6}$	$8.1\cdot 10^{-6}$
$\eta' \to e^+e^-$	—	$1.1\cdot 10^{-9}$	$4.9\cdot 10^{-9}$

and an experiment in which they were measured with sufficient accuracy would therefore be of interest.

The pion form factor

At the present time, the pion electromagnetic form factor has been measured in the interval $-10\ \text{GeV}^2 \leqslant t \leqslant 10\ \text{GeV}^2$ (see, for example, Refs. 39–42). In recent years, a large number of very accurate data for $F_\pi(t)$ have been obtained in the timelike region in experiments at the facilities with colliding electron–positron beams at Novosibirsk[40] and Orsay.[41] Moreover, in recent experiments on elastic scattering at energy 300 GeV the NA-7 group working on the pion beam of the SPS at CERN have obtained new reliable data for the pion form factor in the spacelike region at small values of the momentum transfer.[42] These very accurate experimental data make it possible, on the one hand, to determine more accurately the mass and width of the ρ meson, the pion mean-square radius $\langle r_\pi^2 \rangle$, the scattering length a_1^1, and the behavior of the phase curve $\delta_1^1(t)$, and also to determine the parameters of heavier resonances, for example, ρ' (1250) and ρ'' (1600). On the other hand, the reliable experimental data for $F_\pi(t)$ permit the testing of various theoretical models.

We consider the behavior of the pion electromagnetic form factor in the QCM in the spacelike region $t \equiv q^2 = -Q^2 \leqslant 0$, where q is the momentum transfer. The corresponding diagrams are shown in Fig. 8. The contributions from the triangle quark diagram of Fig. 8a and the resonance diagram of Fig. 8b can be expressed in the form

$$F_\pi^{(a)}(t) = \frac{R_{VPP}(w)}{R_{VPP}(0)};$$
$$F_\pi^{(b)}(t) = \frac{R_{VPP}(w)}{R_{VPP}(0)} \frac{wR_V(w)}{w_\rho R_V(w_\rho) - wR_V(w)}, \qquad (62)$$

where $w = t/\Lambda^2$, $w_\rho = m_\rho^2/\Lambda^2$. The functions $R_{VPP}(w)$ and $R_V(w)$ are given in Table I. The pion form factor is described by the relation

$$F_\pi(t) = F_\pi^{(a)}(t) + F_\pi^{(b)}(t) = \frac{R_{VPP}(w)}{R_{VPP}(0)} \frac{w_\rho R_V(w_\rho)}{w_\rho R_V(w_\rho) - wR_V(w)}. \qquad (63)$$

In the case in which the quark loops do not depend on the momentum, the expression (63) is identical to the corresponding expression for the pion form factor in the VDM.

It is of interest to compare the contributions from the diagrams of Figs. 8a and 8b to the pion electromagnetic radius:

$$\left.\begin{aligned} \langle r_\pi^2 \rangle^{(a)} &= 6 \frac{R'_{VPP}(0)}{R_{VPP}(0)} = \frac{6}{m_\rho^2}\left[\frac{w_\rho}{3B_0}\right] = 0.15\ \text{F}^2; \\ \langle r_\pi^2 \rangle^{(b)} &= \frac{6}{m_\rho^2} \frac{R'_V(0)}{R_V(w_\rho)} = 0.28\ \text{F}^2; \\ \langle r_\pi^2 \rangle &= \langle r_\pi^2 \rangle^{(a)} + \langle r_\pi^2 \rangle^{(b)} = 0.43\ \text{F}^2. \end{aligned}\right\} \qquad (64)$$

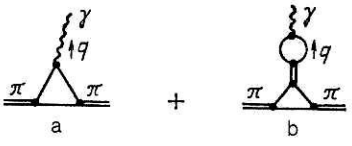

FIG. 8. Quark diagrams that describe the pion electromagnetic form factor.

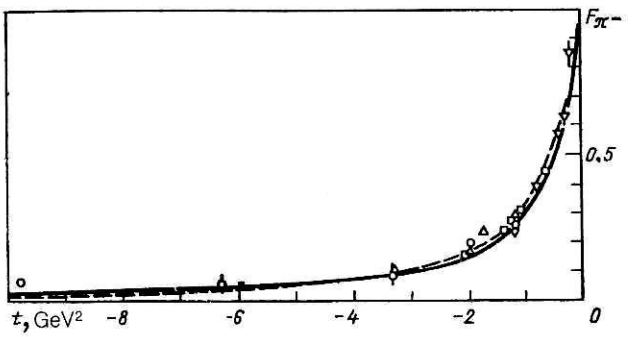

FIG. 9. Pion form factor in the spacelike region. The continuous curve corresponds to the QCM, and the broken curve to the QCD sum rules[43]; the points represent a compilation of experimental data from Ref. 44.

Thus, owing to the allowance for the quark structure of the pion, the resonance diagram gives a value smaller than the VDM prediction ($\langle r_\pi^2 \rangle_{\text{VDM}} = 0.39\ \text{F}^2$). However, the contribution from the triangle diagram plays an important part. Our result is in good agreement with recent experimental data[87]: $\langle r_\pi^2 \rangle = (0.439 + 0.030)\ \text{F}^2$.[87]

The behavior of the pion form factor in the spacelike region ($0 \leqslant Q^2 \equiv -t \leqslant 10\ \text{GeV}^2$) is shown in Fig. 9. It can be seen that the experimental data are described fairly well. Note that the diagram of Fig. 8b is dominant at large values of the momentum transfer, $Q^2 \gtrsim 2\ \text{GeV}^2$.

To describe the behavior of the form factor in the timelike region $t > 0$, it is necessary to take into account the next approximation in $1/N_c$, which leads to the appearance of an imaginary part in the pion form factor, corresponding to the two-particle threshold singularity. In the present paper, we restrict ourselves to the simplest case, namely, to obtain the total propagator of the ρ meson we shall sum not only the single-loop diagrams (see Fig. 6a) but also the imaginary part of the diagram of Fig. 10. On the mass shell of the ρ meson, the imaginary part of the diagram of Fig. 10 is directly related to the $\rho \to \pi\pi$ decay width. Therefore, for the pion form factor we have the modified Breit–Wigner formula

$$F_\pi(t) = \frac{R_{VPP}(w)}{R_{VPP}(0)} \frac{w_\rho R_V(w_\rho) - iJ(w)}{w_\rho R_V(w_\rho) - wR_V(w) - iJ(w)}; \qquad (65)$$

$$J(w) = \frac{\pi}{12}\left[1 - \frac{4w_\pi}{w}\right]^{3/2} w \left[\frac{R_{VPP}(w)}{R_{VPP}(0)}\right]^2. \qquad (66)$$

Accordingly,

$$\operatorname{Re} F_\pi(t) = \frac{R_{VPP}(w)}{R_{VPP}(0)} \times \frac{[w_\rho R_V(w_\rho)(w_\rho R_V(w_\rho) - wR_V(w)) + J^2(w)]}{[w_\rho R_V(w_\rho) - wR_V(w)]^2 + J^2(w)}; \qquad (67)$$

$$\operatorname{Im} F_\pi(t) = \frac{R_{VPP}(w)}{R_{VPP}(0)} \frac{wR_V(w) J(w)}{[w_\rho R_V(w_\rho) - wR_V(w)]^2 + J^2(w)}. \qquad (68)$$

The results of numerical calculations in accordance with Eqs. (67) and (68) are given in Fig. 11. For comparison, we give calculations with the modified function (66):

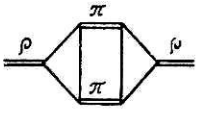

FIG. 10. Diagram that describes the mass operator of the ρ meson in the second approximation in $1/N_c$.

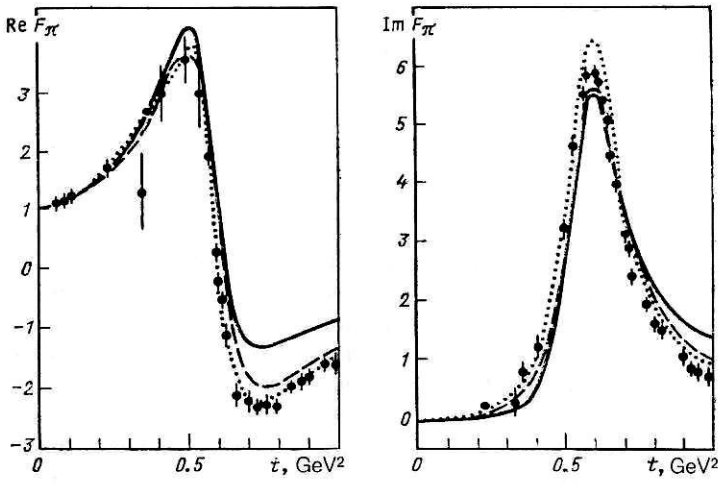

FIG. 11. Real and imaginary parts of $F_\pi(t)$. The continuous and broken curves represent the calculations with $J(w)$ in the form (66) and (69), respectively; the black circles are the results of dispersion approaches[45]; the dotted curve is the result of analysis of the experimental data in the Gounaris–Sakurai model.[46]

$$\tilde{J}(w) = \left(\frac{w_\rho}{w}\right) J(w). \tag{69}$$

Note that the expressions (66) and (69) differ in the behavior off the mass shell of the ρ meson:

$$m_\rho \Gamma_\rho(w_\rho) \to \sqrt{t}\,\Gamma_\rho(\sqrt{t});$$
$$m_\rho \Gamma_\rho(m_\rho) \to m_\rho \left(\frac{m_\rho}{\sqrt{t}}\right) \Gamma_\rho(\sqrt{t}).$$

In this paper, the expressions (66) and (69) are regarded only as the simplest possibilities for taking into account the imaginary part of the pion form factor. The final result must be obtained only after calculation of all the diagrams in the first approximation in $1/N_c$.

Thus, although we have restricted ourselves here to just the single-loop approximation and the simplest approximation for the propagator of the ρ meson, our calculations agree quite well up to $t \simeq 0.8$ GeV^2 with the results of the analysis of the experimental data on $F_\pi(t)$ in the framework of dispersion relations[45] and in accordance with the improved model of Gounaris and Sakurai with allowance for ρ–ω interference.[46]

In Fig. 12 we compare the numerical calculations for $|F_\pi(t)|^2$ with recent experimental data.[40] The predictions of the QCM for $|F_\pi(t)|^2$ agree quite well with the experimental data of Ref. 40 up to $\sqrt{t} \simeq 1.3$ GeV.

It is known that by virtue of the unitarity condition the phase $\delta_\pi(t)$ of the pion electromagnetic form factor

$$\tan \delta_\pi(t) = \frac{\operatorname{Im} F_\pi(t)}{\operatorname{Re} F_\pi(t)} \tag{70}$$

is exactly equal to the phase shift δ_1^1 of elastic $\pi\pi$ scattering in the interval $4m_\pi^2 \leqslant t \leqslant 16m_\pi^2$. However, because the inelasticity parameter $\eta_1^1(t)$ differs little from unity up to $t \simeq 2$ GeV^2, we can assume that

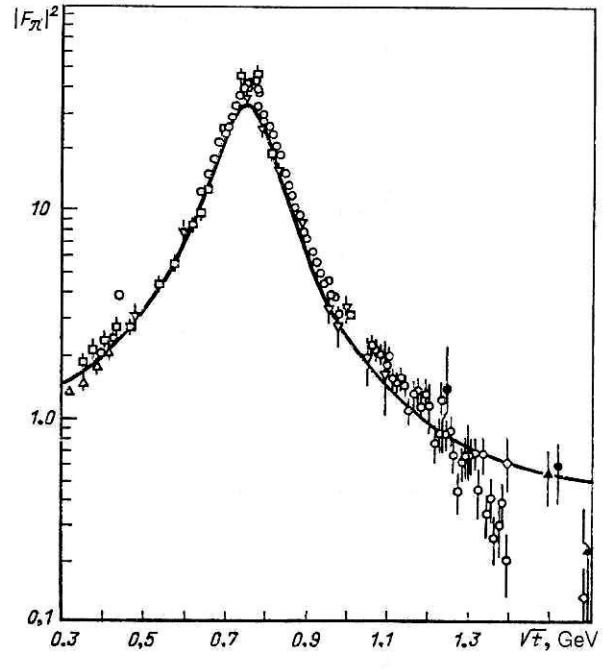

FIG. 12. Behavior of $|F_\pi(t)|^2$ in the interval $0.3 \leqslant \sqrt{t} \leqslant 1.6$ GeV. The continuous curve represents the QCM, and the points are the experimental data taken from Ref. 40.

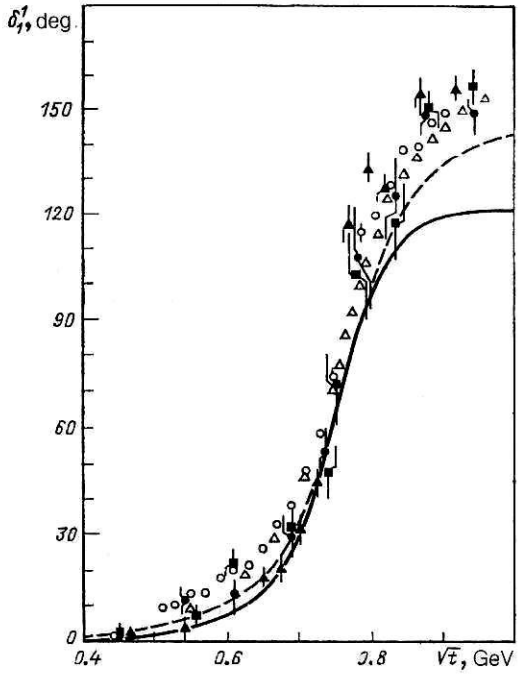

FIG. 13. Phase shifts δ_1^1 of $\pi\pi$ scattering. The continuous curve represents the QCM, and the points are the experimental data: Ref. 47 (open circles), Ref. 48 (open triangles), and Ref. 49 (black circles, triangles, and squares).

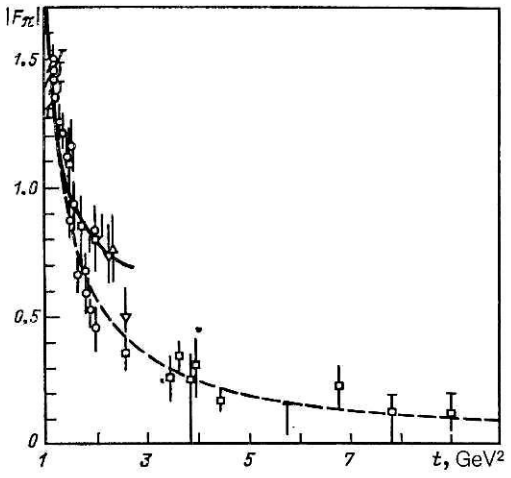

FIG. 14. Behavior of $|F_\pi(t)|$ for $1 \leqslant t \leqslant 10$ GeV^2. The continuous and broken curves represent the calculation with $J(w)$ in the form (66) and (69), respectively; the points are a compilation of experimental data from Ref. 40.

$$\delta_1^1(t) = \delta_\pi(t) \tag{71}$$

in a wider interval of t (see, for example, Ref. 45). We shall use (70) and, in accordance with (67) and (68), calculate the phase shift $\delta_1^1(t)$ of elastic $\pi\pi$ scattering. The numerical results are shown in Fig. 13. One can say that the QCM gives a completely satisfactory description of the experimental values for $\delta_1^1(t)$ up to $\sqrt{t} \simeq 0.8$ GeV.

It is interesting to note that in the case of (69) the predictions of the QCM for $|F_\pi(t)|$ agree remarkably well with experiment up to $t \simeq 10$ GeV^2 (Fig. 14).

We regard these results as preliminary. First, it is necessary to make systematic calculations in the second approximation in $1/N_c$ and, second, the treatment must include heavier resonances, for example, the ρ' meson. Such work is planned for the future.

The decay $\pi^- \to e\nu\gamma$

The electroweak decay $\pi^- \to e\nu\gamma$ is interesting above all because the structure-dependent part of the amplitude is characterized by two form factors:

$$M_{SD}^{\mu\nu}(p, q) = [g^{\mu\nu} pq - p^\mu q^\nu] f_A(q^2) - i\varepsilon^{\mu\nu\alpha\beta} p^\alpha q^\beta f_V(q^2), \tag{72}$$

where p and q are the momenta of the pion and photon, respectively. The experimentally measured quantity is

$$\gamma = f_A(0)/f_V(0). \tag{73}$$

Until recently, the experiments gave with equal probability two values for γ with opposite signs[50]:

$$\gamma = 0.44 \pm 0.12 \quad \text{or} \quad \gamma = -2.36 \pm 0.12.$$

Recent experiments made at SIN[51,52] and at LAMPF[53] have permitted the choice of the positive value of γ (see Table XI).

The process $\pi^- \to e\nu\gamma$ has been considered in many theoretical studies (see the review of Ref. 55). The predictions for the values of γ are varied, and at times contradictory. A particular situation has arisen in relativistic quark models.[56,57,96] It has been found that if a restriction is made

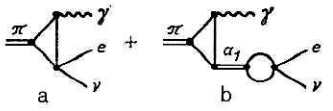

FIG. 15. Diagrams that describe the structure-dependent part of the $\pi \to e\nu\gamma$ decay amplitude.

in the description of the decay $\pi^- \to e\nu\gamma$ to a diagram like that of Fig. 15a, then $\gamma = 1$. Additional assumptions are required in order to obtain a different value of γ. In our view, the most natural assumption from the physical point of view appears to be that of the need to take into account an intermediate $a_1(1275)$ meson[56,96] in the description of this process. Allowance for the a_1 meson in the relativistic quark models leads to the appearance of an additional diagram of the type shown in Fig. 15b. It should be emphasized that the quark loop corresponding to the transition $a_1 \to e\nu$ contains in the local limit a quadratic divergence, in contrast to the diagram of Fig. 15a, which contains only a logarithmic divergence. Therefore, the standard prescriptions for taking into account divergences that are adopted in the relativistic quark models[56,57] are not valid in their direct form.

In the QCM, the calculation of the diagrams of Fig. 15 does not present difficulties. As a result of the calculations, we obtain

$$\gamma = 1 - \frac{2h_A}{w_A}\left[\frac{2A_0B_0}{a_0} - B_1\right] = 0.78. \tag{74}$$

It can be seen that this value is in agreement with the recent experimental data and with the results of Ref. 58 ($\gamma = 0.7$).

In connection with the important contribution of the intermediate a_1 meson to the axial form factor in $\pi^- \to e\nu\gamma$, it is of interest to calculate the observable characteristics of the a_1 meson. We consider the strong decay $a_1 \to \rho\pi$ and the radiative decay $a_1 \to \pi\gamma$. The corresponding diagrams are shown in Fig. 16. The matrix element of the decay $a_1 \to \rho\pi$ can be expressed in the form

$$M^{\mu\nu}(q_1, q_2) = g^{\mu\nu} g_1^A(w_A) + [g^{\mu\nu} q_1 q_2 - q_1^\mu q_1^\nu] g_2^A(w_A, w_\rho), \tag{75}$$

where

$$g_1^A(w_A) = \Lambda \frac{4\pi}{\sqrt{6}} \sqrt{h_A h_\rho h_\pi}\, R_P(w_A);$$

$$g_2^A(w_A, w_\rho) = \frac{1}{\Lambda} \frac{4\pi}{\sqrt{6}} \sqrt{h_A h_\rho h_\pi}\, \frac{w_A R_{PVV}(w_A) - w_\rho R_{PVV}(w_\rho)}{w_A - w_\rho}.$$

Experimental measurements have been made both of the $a_1 \to \rho\pi$ decay width and of the ratio G_D/G_S, which characterizes the relative contributions of the D and S waves. The quantities G_D and G_S are related to $g_{1,2}^A$ in (75) in the standard way.[60] It can be seen from Table VI that the $a_1 \to \rho\pi$ decay width is somewhat greater than the present experi-

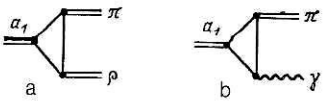

FIG. 16. Diagrams that describe the decays $a_1 \to \rho\pi$ (a) and $a_1 \to \pi\gamma$ (b).

TABLE VI. Widths of the decays $a_1 \to \rho\pi$ and $a_1 \to \pi\gamma$ and ratio of the axial and vector form factors in the decay $\pi \to e\nu\gamma$.

Process	Observed quantity	QCM	Experiment (references in square brackets)	
$a_1 \to \rho\pi$	Γ, MeV	498	345±45	[38]
	$D=G_D/G_S$	$2.6\cdot10^{-3}$	~ 0	[61]
$a_1 \to \pi\gamma$	Γ, keV	518	640±246	[38]
$\pi \to e\nu\gamma$	$\gamma=f_A(0)/f_V(0)$	0.78	0.52±0.06	[51]
			0.7±0.5	[52]
			0.39±0.06	[53]
			0.67±0.09±0.16	[54]

mental value. The small value of the ratio G_D/G_S agrees with the experimental data,[61] indicating the absence of a D-wave contribution to $\Gamma(a_1 \to \rho\pi)$. It should be noted that in the description of the decay $a_1 \to \rho\pi$ an important part is played by nondiagonal π–a_1 transitions,[58] which we do not consider in this paper. Allowance for them will evidently reduce the $a_1 \to \rho\pi$ decay width.[58,59]

The matrix element of the decay $a_1 \to \pi\gamma$ is determined by the diagrams of Fig. 16b and has the gauge-invariant form

$$M(a_1 \to \pi\gamma) = \varepsilon^\mu(p)\varepsilon^\nu(q)\, i e [g^{\mu\nu} pq - p^\nu q^\mu] \frac{g_{a_1\pi\gamma}}{m_{a_1}^2},$$

where the constant $g_{a_1\pi\gamma}$ is related to the functions $g_{1,2}^A$ in (75) (see Ref. 59). The result of the calculations for the $a_1 \to \pi\gamma$ decay width is given in Table VI. The existing experimental data are not at all accurate, and therefore this result can be regarded as a prediction.

Electromagnetic radii of kaons and parameters of the K_{l_3} decay

The electromagnetic form factors of the charged and neutral kaons are determined by the diagrams of Fig. 17 and can be expressed in the form

$$F_{K^+}(t) = F_\Delta^+(t) + F_\rho(t) + F_\omega(t) - F_\varphi(t),$$
$$F_{K^0}(t) = F_\Delta^0(t) - F_\rho(t) + F_\omega(t) - F_\varphi(t),$$

where $t = q^2$ is the square of the momentum transfer q.

Values for the electromagnetic radii of the kaons, calculated in accordance with the standard relation

$$\langle r_K^2 \rangle = 6 F_K'(0),$$

are given in Table VII. It can be seen that there is agreement with the experimental values.

The decay $K \to \pi l\nu$ (K_{l_3}) is determined by the diagrams of Fig. 18 and can be expressed in the form

$$M^\mu(p_1, p_2) = F_+(t)(p_1 + p_2)^\mu + F_-(t)(p_1 - p_2)^\mu.$$

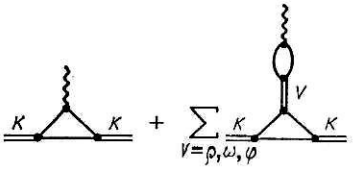

FIG. 17. Diagrams that describe the kaon electromagnetic form factor.

Using the standard parametrization for the form factors,[29]

$$F_\pm(t) = F_\pm(0)\left[1 + \lambda_\pm \frac{t}{m_\pi^2}\right],$$

we determine the parameters of K_{l_3} decay:

$$\lambda_\pm = \frac{m_\pi^2}{F_\pm(0)} F_\pm'(0),$$
$$\xi(0) = F_-(0)/F_+(0).$$

Their values are given in Table VII. It is of interest to verify the Callan–Treiman–Okubo–Pandit relation[29]:

$$F_+(m_K^2) + F_-(m_K^2) = f_K/f_\pi. \qquad (76)$$

For this, it is sufficient to calculate the values of the form factors $F_\pm(t)$ at the point m_K^2. It was found that

$$F_+(m_K^2) + F_-(m_K^2) = 0{,}9\, f_K/f_\pi,$$

i.e., the relation (76) holds with 10% error.

6. THE PART PLAYED BY SCALAR MESONS IN LOW-ENERGY PHYSICS

The scalar 0^{++} mesons play an important part in low-energy hadron physics. Linear realization of chiral symmetry required the introduction of σ particles,[29] and this proved to be very convenient for the construction of phenomenological chiral Lagrangians describing the low-energy relations of current algebra. Phenomenological analysis and model studies[11,62] of processes that admit the existence of intermediate scalar states ($\pi\pi$ scattering, pion polarizability, the decays $K \to 2\pi$, $K \to 2\gamma$, etc.) showed that the description of the experimental data required the introduction of an ε meson (or σ meson) with mass 600–800 MeV. Reliable experimental data indicating its existence are as yet absent. The existence of the following low-energy scalar states has up to now been experimentally established: $a_0(980)$, $f_0(975)$, $f_0(1300)$, $K_0^*(1350)$. For some of them the partial widths have been measured.

From the point of view of their quark composition, the assumption that the scalar mesons are two-quark states does not conflict with modern experimental data, although there are investigations[63] in which scalar mesons are treated as four-quark systems. In addition, one cannot rule out the possibility that the singlet 0^{++} states are mixtures of quark and gluon states.[64]

In the approach which we have developed, we shall regard the scalar mesons ($a_0, f_0, \varepsilon, K_0^*$) as two-quark states described by the Lagrangian (46).

TABLE VII. Electromagnetic radius of the kaon and parameters of the K_{l_4} decay.

Quantity	QCM: Contributions of individual diagrams					Experiment (references in square brackets)
	Δ	ρ	ω	φ	Sum	
$\langle r^2\rangle_{K^+}$, F^2	0.10	0.078	0.026	−0.027	0.18	0.26±0.07 [38]
$\langle r^2\rangle_{K^0}$, F^2	0.009	−0.078	0.026	−0.027	−0.07	−0.05±0.026 [88] 0.08±0.05 [89]
λ_+	0.037					0.029±0.004 [90]
λ_0	0.0034					0.0032±0.0099 [38]
$\xi(0)$	−0.39					−0.35±0.14 [38]

In accordance with the low-energy phenomenology, we shall regard the mass of the ε meson and the mixing angle as free parameters.

We discuss in more detail the choice of the matrix $\Gamma_S = I - iH(\hat{\partial}/\Lambda)$, which determines the 0^{++} quantum numbers. To this end, we consider the diagram of Fig. 2b (in which $\Gamma_1 = \Gamma_S$, $\Gamma_2 = \Gamma_3 = \gamma^5$), which describes the decay $S \to PP$. The corresponding structure integral, calculated for zero masses of the final states and normalized to unity at $m_S = 0$, can be expressed in the form

$$\left.\begin{aligned} I_H(w_S) &= [I_0(w_S) - 4HI_1(w_S)]/I_H(0); \\ I_0(w) &= A_0 - w\int_0^1 dua\left(-u\frac{w}{4}\right) \\ &\quad\times\left[\frac{1}{2}\ln\frac{1+\sqrt{1-u}}{1-\sqrt{1-u}} - \sqrt{1-u}\right]; \\ I_1(w) &= B_1 + \frac{w^2}{32}\int_0^1 duub\left(-u\frac{w}{4}\right) \\ &\quad\times\left[\frac{1}{2}\ln\frac{1+\sqrt{1-u}}{1-\sqrt{1-u}} - \sqrt{1-u}\right]. \end{aligned}\right\} \quad (77)$$

Figure 19 gives graphs of $I_H(w_S)$ as a function of the mass m_S for different values of H. It can be seen that in the case $H = 0$ the function $I_0(w_S)$ vanishes at $m_S \simeq 1070$ MeV. Such a dependence for $H = 0$ has the consequence that the theoretical value of the $f_0(975) \to \pi\pi$ decay width is much lower ($\Gamma \simeq 1$ MeV) than the experimental value $\Gamma_{\text{exp}} = 26 \pm 5$ MeV.

This result, corresponding to the simplest choice of the scalar two-quark current with $\Gamma_S = I$, apparently indicates a more complicated structure of the scalar mesons. It is entirely possible that a four-quark component of the quark current plays an important part in the scalar mesons (for a detailed analysis of this problem, see Ref. 63). We intend to make such an analysis in the future. In the present paper we restrict ourselves to inclusion of the additional two-quark interaction with a derivative as expressed in (46), and we shall regard H as a free parameter.

As a basis to fit the parameters H, δ_S, and m_ε, which characterize the scalar mesons as two-quark states, we take, first, Adler's self-consistency condition,[29] which requires vanishing of the $\pi\pi \to \pi\pi$ and $\pi^0\gamma \to \pi^0\gamma$ amplitudes in the limit $m_\pi \to 0$ (Fig. 20), and second, the experimental values of the $a_0 \to \pi\pi$ decay width and of the s-wave $\pi\pi$ scattering lengths: a_0^0 and a_0^2. The self-consistency condition can be expressed in the form

$$5b_0 = 2\Lambda^2\cos\delta_S a_0[A_0 - 4HB_1] \times(5\cos\delta_S - \sqrt{2}\sin\delta_S)\, h_\varepsilon D_\varepsilon(0); \quad (78a)$$

$$B_0 = 2\Lambda^2\cos^2\delta_S[A_0 - 4HB_1]^2 h_\varepsilon D_\varepsilon(0), \quad (78b)$$

where a_0, b_0, A_0, B_0, and B_1 are parameters of the model [see (55)]. To make the fit, it is convenient to use the quotient of Eqs. (78b) and (78a), which does not contain the mass of the ε meson, and to consider the ratio

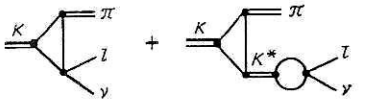

FIG. 18. Diagrams that describe the decay $K \to \pi l\nu$.

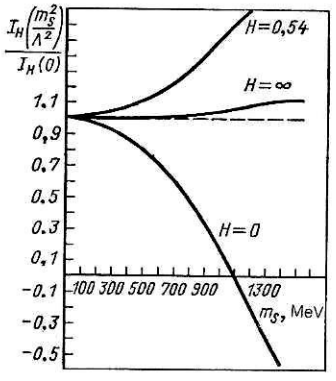

FIG. 19. Graphs of the dependence of the structure integral $I_H(m_S^2/\Lambda^2)$, which determines the decay $S \to PP$, on the mass m_S of the scalar meson for different values of the parameter H.

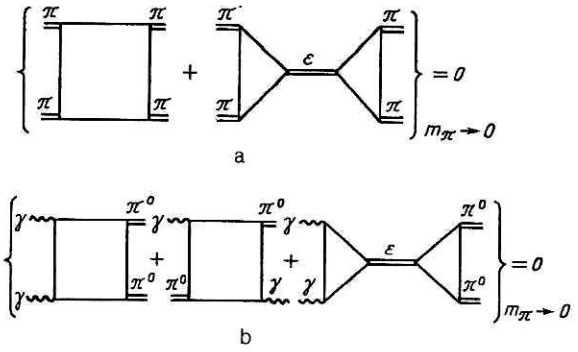

FIG. 20. Adler's self-consistency condition.

$$R=\frac{5b_0\cos\delta_S\,[A_0-4HB_1]}{B_0a_0\,(5\cos\delta_S-\sqrt{2}\sin\delta_S)}=1, \tag{79}$$

which contains only the parameters H and δ_S.

The matrix element corresponding to the decay $f_0\to\pi\pi$ is

$$g_{f_0\pi\pi}=4\sin\delta_S\Lambda h_\pi\sqrt{\frac{h_{f_0}}{6}}\,[I_0(w_S)-4HI_1(w_S)]$$

and, accordingly, the decay width is

$$\Gamma(f_0\to\pi\pi)=\frac{3}{32\pi}\,m_{f_0}\sqrt{1-\frac{4m_\pi^2}{m_{f_0}^2}}\,\frac{g_{f_0\pi\pi}^2}{m_{f_0}^2}. \tag{80}$$

Figure 21 shows graphs of the quantities

$$R\,(H,\ \sin\delta_S)\text{and}\,Q\,(H,\ \sin\delta_S)=\frac{\Gamma^{\text{th}}(f_0\to\pi\pi)}{\Gamma^{\text{exp}}(f_0\to\pi\pi)}$$

as functions of H for different values of $\sin\delta_S$. The optimal values of the parameters H and $\sin\delta_S$, at which the values of R and Q are near unity, are

$$H=0.55;\quad \sin\delta_S=0.3;\quad \delta_S=17^\circ. \tag{81}$$

We determine the mass of the ε meson from the condition of best fit of the s-wave $\pi\pi$ scattering lengths a_0^0 and a_0^2 to the existing experimental data.[65] The $\pi\pi$ scattering amplitude is described by the diagrams of Fig. 22. Figure 23 shows a_0^0 and a_0^2 as functions of the mass of the ε meson. It can be seen that the best agreement with the existing experimental data is achieved when

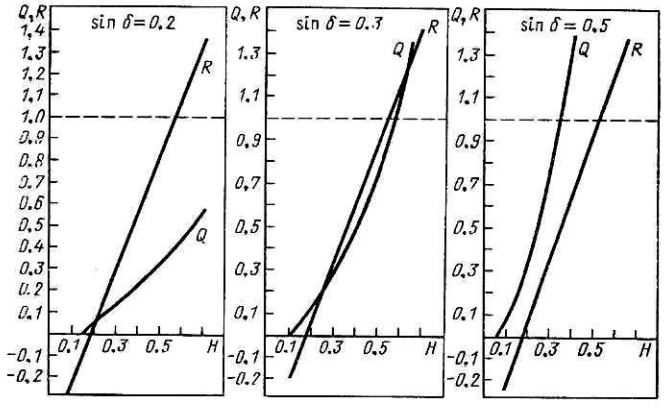

FIG. 21. Graphs of $R(H, \sin\delta_S)$ and $Q(H, \sin\delta_S)$ as functions of the parameter H for different values of $\sin\delta_S$.

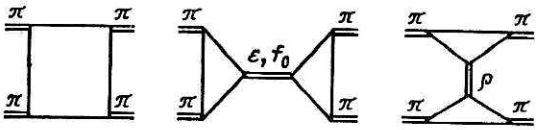

FIG. 22. Diagrams that describe $\pi\pi$ scattering.

$$m_\varepsilon=600\ \text{MeV}.$$

It should be noted that the experimental measurement of the scattering lengths and phase shifts of $\pi\pi$ scattering is a complicated problem, since direct study of $\pi\pi$ scattering is not possible in a direct experiment, and therefore the information is extracted indirectly from other processes [for example, from data on the decay $K\to e\nu\pi\pi$ (Ref. 65) or on $\pi N\to\pi\pi N$ inelastic scattering[66]].

The difficulties in the direct experimental measurement of the $\pi\pi$ scattering lengths and phase shifts stimulate the search for other possibilities of measurement of these quantities with smaller errors. One such experiment is the generation and measurement of the lifetime of atoms formed from π^+ and π^- mesons, $A_{2\pi}$, as was proposed in Ref. 68. The probability of decay of the $A_{2\pi}$ atom into two π^0 mesons is determined by the expression[69]

$$W[A_{2\pi}\to\pi^0\pi^0]=\frac{16\pi}{9}\left[\frac{2\,(m_{\pi^+}-m_{\pi^0})}{m_\pi}\right]^{1/2}|a_0^0-a_0^2|^2|\Psi(0)|^2,$$

where a_0^0 and a_0^2 are the s-wave $\pi\pi$ scattering lengths with isospin 0 and 2, respectively, and $\Psi(0)$ is the value of the wave function of the ground state of the atom at the origin. In the experiment of Ref. 68 independent measurements could be made of $\Psi(0)$ and of the lifetime of the $A_{2\pi}$ atom, and this made it possible to determine directly the difference of the $\pi\pi$ scattering lengths. The basic possibility of a measurement of the shift of the $2S$–$2P$ levels was also demonstrated.

As was shown by the calculations of Ref. 70, the value of the wave function at the origin, $\Psi(0)$, differs little from the corresponding Coulomb value. Therefore, the lifetime of the $A_{2\pi}$ atom is determined by the difference of the s-wave $\pi\pi$ scattering lengths. Table VIII gives the values of the lifetime calculated both in the framework of the QCM and in other approaches. Measurement of the lifetime of the $A_{2\pi}$ atom permits more accurate determination of the mass of the intermediate ε meson. The widths of the strong and radiative decays of the scalar mesons are given in Table IX. They were calculated with the values of the parameters H, $\sin\delta_S$, and

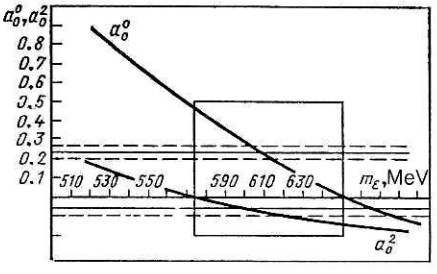

FIG. 23. Graphs of the s-wave $\pi\pi$ scattering lengths as functions of the mass of the ε meson.

TABLE VIII. The s-wave $\pi\pi$ scattering lengths and the lifetime of the $A_{2\pi}$ atom.

Property	Experiment		Current algebra	Model of superconducting current (Ref. 91)	QCM
	Ref. 65	Ref. 66			
a_0^0 $(m_\pi=1)$	0.26±0.05	0.23±0.03	0.20	0.29	0.28
a_0^2 $(m_\pi=1)$	−0.028±0.012	−0.06±0.07	−0.06	−0.025	−0.054
τ $(A_{2\pi})$, 10^{-15} c	2.6±0.9	2.5±1.3	3.1	2.1	1.9

m_ε obtained above. Among the considered decays, only the decay $f_0 \to \pi\pi$ was used to make the fit. The width of the decay $a_0 \to \eta\pi$ agrees well with experiment.

We now turn to the calculation of the electric and magnetic polarizabilities of the π^+ and π^0 mesons. The values of these parameters are extracted from the amplitude for Compton scattering of a photon by a π meson. The matrix element of the process $\pi\gamma \to \pi\gamma$ on the photon mass shell is expressed in general form as follows[71]:

$$M_{\mu\nu}(\pi\gamma \to \pi\gamma) = -\sum_{a=1}^{2} T^a_{\mu\nu} F_a(s,\ t), \tag{82}$$

where

$$T^1_{\mu\nu} = (q_1p_1)\, q_{2\mu}p_{2\nu} + (q_2p_2)\, q_{1\nu}p_{1\mu} - g_{\mu\nu}\,(p_1q_1)\,(p_2q_2) - p_{1\mu}p_{2\nu}\,(q_1q_2);$$

$$T^2_{\mu\nu} = g_{\mu\nu}q_1q_2 - q_{1\nu}q_{2\mu};$$

$F_{1,2}(s, t)$ are form factors determined by the internal structure of the π mesons; q_1 and q_2 are the momenta of the initial and final photons; p_1 and p_2 are the momenta of the initial and final π mesons; and

$$s = (p_1 + q_1)^2 = (p_2 + q_2)^2;$$
$$t = (p_1 - p_2)^2 = (q_1 - q_2)^2.$$

It can be shown[71] that the electric and magnetic polarizabilities of the π mesons are connected to the form factors $F_{1,2}$ by the relations

$$\left.\begin{aligned} \alpha_\pi &= -\frac{F_1(m_\pi^2,\ 0) + F_2(m_\pi^2,\ 0)}{m_\pi} \\ \beta_\pi &= F_2(m_\pi^2,\ 0)/m_\pi. \end{aligned}\right\} \tag{83}$$

In Table X we give diagrams that determine the amplitude of the process $\pi\gamma \to \pi\gamma$. Besides the box diagrams, we take into account diagrams with intermediate scalar, vector, and axial-vector mesons. Note that only the diagrams with intermediate vector and axial-vector mesons contribute to F_1. The form factors $F_{1,2}(m_\pi^2, 0)$ can be expressed in the form

$$\left.\begin{aligned} F_1(m_\pi^2,\ 0) &= F^V(m_\pi^2,\ 0) + F_1^A(m_\pi^2,\ 0); \\ F_2(m_\pi^2,\ 0) &= F^{\mathrm{BOX}}(m_\pi^2,\ 0) + F^S(m_\pi^2,\ 0) \\ &+ F_2^A(m_\pi^2,\ 0) - F^V(m_\pi^2,\ 0). \end{aligned}\right\} \tag{84}$$

Substituting (84) in (83), we obtain the values of the electric and magnetic polarizabilities of the π^+ and π^0 mesons. Table X gives the contributions to them from the various diagrams and the total values of these parameters for $m_\varepsilon = 600$ MeV. The main contribution to the π^+ polarizability is made by the diagrams with intermediate scalar mesons. The small value of the electric polarizability of the π^0 meson is due to the mutual cancellation of the contributions from the box diagram and the diagrams with intermediate scalar mesons, in accordance with the self-consistency condition (78). However, complete cancellation does not occur because we take into account not only the $\varepsilon(600)$ meson but also the f_0 (980) meson. Besides the scalar intermediate states, we also considered vector and axial-vector intermediate mesons. The intermediate $\omega(780)$ and $f_1(1285)$ mesons play an im-

TABLE IX. Widths of strong and radiative decays of scalar mesons.

Process	QCM	Experiment[38]
$f_0 \to \pi\pi$	22 MeV	(26±5) MeV
$a_0 \to \eta\pi$	56 MeV	(54±7) MeV
$\varepsilon \to \pi\pi$	360 MeV	—
$f_0 \to \gamma\gamma$	0.37 keV	<0.8 keV
$a_0 \to \gamma\gamma$	0.41 keV	$(0.19\pm0.07^{\pm0.1}_{-0.07})$ keV
$\varepsilon \to \gamma\gamma$	0.33 keV	—

TABLE X. Polarizability of pions, in 10^{-43} cm^3.

Diagram	α_{π^+}	α_{π^0}	β_{π^+}	β_{π^0}
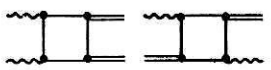	−0.615	−6.15	0.615	6.15
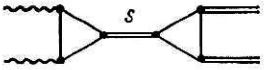	6.55	6.55	−6.55	−6.55
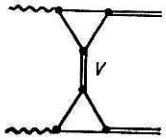	—	—	0.26	1.7
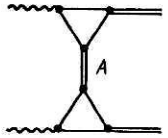	−0.163	−1.46	0.115	1.5
Result	5.77	−1.06	−5.56	2.8
Experiment[92]	6.8±1.4±1.8	—	—	—
Experiment[93]	—	< 35	—	—

portant part in the description of the π^0 polarizability.

The value that we have obtained for α_{π^+} is close to the value of Ref. 72. We obtain a positive value $\alpha_{\pi^+} + \beta_{\pi^+} = 0.21 \times 10^{-43}$ cm^3, in agreement with the result obtained in the approach based on the use of dispersion sum rules.[73] The nonzero value of this quantity is due to the contribution of the pseudovector and vector states.

Thus, we have calculated the electric and magnetic polarizabilities of the π^+ and π^0 mesons in the Quark Confinement Model. In the calculation of the matrix element of the process $\pi\gamma \to \pi\gamma$ we have taken into account diagrams with intermediate scalar, vector, and axial-vector states. We have found that the diagrams with an intermediate $\varepsilon(600)$ meson play the main part in the calculation of α_π and β_π. Our results are in satisfactory agreement with the experimental data and do not conflict with the results obtained in the framework of other approaches.

Our analysis of many-particle processes with the participation of intermediate particles has shown that scalar 0^{++} mesons, in particular the $\varepsilon(600)$ meson, play an important part in their description. We have found that when the scalar mesons are treated in the framework of the QCM as two-quark states some nontrivial questions arise. For example, the choice of the two-quark current with quantum numbers 0^{++} in the simplest form without derivatives, $J_{0^{++}} = -\bar{q}Iq$, does not permit us to obtain the correct value for the width of the observed decay $f_0 \to \pi\pi$. Therefore, we have considered a more general form of the scalar 0^{++} current with a derivative, $J_{0^{++}} = \bar{q}[I - iH\overleftrightarrow{\partial}/\Lambda]q$, where H is an additional free parameter. By means of this form of the scalar vertex, we have obtained a description of the experimental data for the s-wave $\pi\pi$ scattering length, the pion polarizabilities, and the widths of the observable decays of scalar mesons, and we have also verified the main low-energy relations of chiral theories for the amplitudes of $\pi\pi$ and $\pi\gamma$ scattering.

Naturally, the introduction of the additional term with a derivative in the case of scalar mesons cannot be regarded as the final solution to the problem of the scalar mesons. In particular, similar terms with a derivative also arise in the case of other mesons (for example, when allowance is made for nondiagonal π–a_1 transitions[11]). One can hardly hope to achieve a complete description of low-energy meson physics by the approximation of the total gluon Green's function in (10) by the δ function (7). This approximation leads to a Lagrangian of Nambu–Jona-Lasinio type. It is necessary to consider the more general form (11) for the gluon Green's function and use it to solve equations of Bethe–Salpeter type for the bound states of quarks. We plan such work for the future.

Thus, our analysis has shown, first, that to describe many-particle processes ($\pi\pi \to \pi\pi$, $\pi\gamma \to \pi\gamma$) in the QCM we require the light scalar $\varepsilon(600)$ meson. This is in agreement with other approaches.[11,29,62] Second, the results obtained for the decay widths of the scalar mesons and for the mixing angle can be regarded as an indirect indication that the scalar mesons have a more complicated nature than that of the simplest two-quark state.

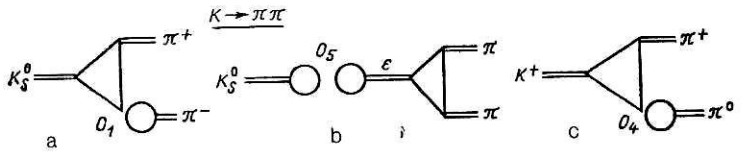

FIG. 24. Diagrams that describe the decay $K \to 2\pi$.

7. NONLEPTONIC DECAYS OF K MESONS

Kaon physics is exceptionally rich in interesting physical effects. Among them, the nonleptonic decays of kaons are particularly interesting. Study of these processes leads to a deeper understanding of the structure of the weak interactions, and also of the connection between the weak and strong interactions of quarks. In addition, the empirical $\Delta I = 1/2$ rule does not have a complete theoretical explanation, although rather a lot of studies[21] have been devoted to this problem. The rule states that the transitions in which the isospin I is changed by 3/2 are strongly suppressed in comparison with the $\Delta I = 1/2$ transitions. At the present time, two approaches have crystallized in the physics of weak interactions in explaining the $\Delta I = 1/2$ rule.

1) Terms that are products of quark currents are introduced into the Lagrangian in such a way that nonleptonic decays with $\Delta I = 3/2$ are suppressed (see, for example, Ref. 74). This is a purely phenomenological approach and can hardly give information about the weak and strong interactions of quarks.

2) The weak interactions of quarks are described by the standard Weinberg–Salam model with allowance for QCD corrections. Allowance for the strong interaction of the quarks at short distances enhances the $\Delta I = 1/2$ amplitude. However, this enhancement is not sufficient to explain the $\Delta I = 1/2$ rule. One seeks an additional dynamical mechanism to enhance the $\Delta I = 1/2$ transitions; this mechanism is associated with the calculation of the matrix elements of hadron–quark transitions at large distances.

We shall follow the second path. We consider in more detail the weak quark–quark interaction. The effective Hamiltonian of this interaction is obtained in the Weinberg–Salam model with allowance for the gluon QCD corrections associated with the strong interaction of the quarks at short distances and is expressed in the form[75]

$$H_{\text{eff}}^{w} = \frac{G_F}{2\sqrt{2}} \sin\theta_c \cos\theta_c \sum_{i=1}^{6} c_i O_i, \tag{85}$$

where O_i are four-quark local operators.[75] The coefficients c_i depend on the masses of the W boson and the c quark, and also on QCD parameters: the value of the running coupling constant $\alpha_S = g^2(\mu)/4\pi$ and μ, the normalization point.[75]

The main problem is in the calculation of the matrix elements of the operators O_i at low energies. To this end, various models of the strong interactions are used.[21] For example, the nonleptonic decays of kaons have been studied in various quark models,[76–78] in dispersion approaches,[79] and in approaches based on the $1/N_c$ expansion.[80,81] In a number of approaches,[77,83] the method of current algebra has been used to calculate the matrix element of the two-particle decay $K \to 2\pi$. In the studies of Refs. 81 and 83, the method of vacuum insertion was used to calculate the matrix elements of the four-quark operators. However, the use of this method has recently been criticized, for example, in Ref. 84.

A subject of separate discussion is the operator O_5. This operator, which contributes to the amplitudes with $\Delta I = 1/2$, contains not only "left" but also "right" quark currents, in contrast to O_1–O_4, which consist solely of "left" currents. There are two opposite points of view with regard to the part played by O_5 in the explanation of the $\Delta I = 1/2$ rule. In Ref. 83 it is asserted that the operators O_5 and O_6 play the main part in the enhancement of the corresponding amplitudes. In the pioneering study of Ref. 75, and also in Ref. 76, it is noted that the main part is played by the pole contribution from these operators, i.e., the contribution from an intermediate scalar (σ or ε) particle. In contrast, it is shown in Refs. 79 and 85 that the operators O_5 and O_6 cannot give the necessary enhancement of the $\Delta I = 1/2$ amplitudes.

In the quark-loop model,[76] the enhancement of the $\Delta I = 1/2$ amplitudes is due to the large contribution of the diagrams with an intermediate $\varepsilon(770)$ meson. The results obtained in Refs. 78 and 83 depend on a large number of parameters and on the method of calculation. In Refs. 78 and 80, reasonable agreement with experiment is achieved by the introduction of phenomenological corrections to the matrix elements. In Ref. 82, the agreement with experiment is associated with the choice of a correction parameter for the coefficients c_1–c_6. In Ref. 86 the introduction of a new neutral interaction is proposed in order to obtain the amplitudes of the nonleptonic decays. The result depends on the choice of the constant of this interaction ($Ag_A = 30$).

It should be emphasized that the enhancement of the amplitudes of transitions with $\Delta I = 1/2$ in Refs. 78, 80, 82, 83, and 86 is achieved by the introduction of additional phenomenological parameters. Therefore, despite the reasonable agreement with the experimental data obtained in the cited studies, the problem of the $\Delta I = 1/2$ rule cannot be regarded as solved.

We shall also proceed from the Hamiltonian (85), regarding it as an effective Hamiltonian of weak nonleptonic interactions and describing transitions with $\Delta S = 1$. We shall assume that the coefficients c_i are determined by the

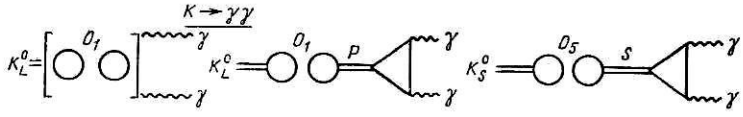

FIG. 25. Diagrams that describe the decay $K \to 2\gamma$.

TABLE XI. Values of the coefficients $\{c_i\}$.

c_i	c_1	c_2	c_3	c_4	c_5
QCM $\mu=0.25$ GeV, $\alpha_S=0.45$	−1.97	0.115	0.093	0.47	−0.036
Ref. 21 $\alpha_S=1$, $m_t=40$ GeV	−2,38	0.10	0.084	0.42	−0.047
Ref. 94 $\alpha_S=0.1$, $\mu=3$ GeV	−3.04	0,32	0.22	1.23	−0.13
Ref. 82 $\alpha_S=1$, $\varepsilon=1.1$, $\Lambda=0.1$ GeV	−5.11	0.02	0.04	0.2	−0.17
Ref. 83 $c_2, c_3, c_4 \to \frac{1}{4}(c_2, c_3, c_4)$, $c_5, c_6 \to 3(c_5, c_6)$	−2.538	−0.0205	0.02	0.1	0.24

relations of Ref. 21, and we shall choose the parameters μ and α_S by a fit to the experimental data.

The diagrams that determine the amplitudes of the decays $K_S^0 \to \pi^+\pi^-$, $K_S^0 \to \pi^0\pi^0$, $K^+ \to \pi^+\pi^0$ are shown in Fig. 24.

The matrix elements of the $\Delta I = 1/2$ decays $K_S^0 \to \pi^+\pi^-$ and $K_S^0 \to \pi^0\pi^0$ are determined as the contact diagrams shown in Fig. 24a and also as the pole diagram with an intermediate ε meson shown in Fig. 24b.

The diagrams that determine the amplitudes of the electromagnetic decays of neutral kaons are shown in Fig. 25. It should be noted that intermediate states play an important part in these decays. The parameters μ and α_S were fitted on the basis of the well-established values of the widths of the decays $K_S^0 \to \pi^+\pi^-$, $K^+ \to \pi^+\pi^-$, and $K_L^0 \to \gamma\gamma$. The numerical values of the coefficients $\{c_i, i = 1,..., 6\}$ obtained as a result of the fit are given in Table XI. For comparison, we give the coefficients used in other approaches. The set of coefficients that we have obtained is closest to the set proposed in Ref. 21.

In Table XII we have collected together the results of the calculations of the $K \to 2\pi$, 2γ decay widths in the QCM and in a number of other approaches. Our results are in good agreement with the experimental data. It should be noted that the $K_S^0 \to \gamma\gamma$ decay width has been calculated with the parameters already fixed and is therefore a test for the assumptions that were made. The value obtained for the width of this decay is in agreement with the recently measured experimental value.

It is of interest to elucidate the part played by the various operators in enhancing the amplitudes of the $\Delta I = 1/2$ processes. In Table XIII we give the relative contributions to $M(K_S^0 \to \pi^+\pi^-)$ from the various operators O_i with allowance for the coefficients c_i: $M_{O_1-O_4}$ is the contribution from the operators O_1–O_4; $M_{O_5}^K$ is the contribution from the contact diagram with O_5; and $M_{O_5}^{\varepsilon}$ is the contribution from the pole diagram with O_5 (the diagram with an intermediate ε meson). As we have already noted, there are two opposed points of view with regard to the part played by the operator O_5 in the enhancement of the amplitudes with $\Delta I = 1/2$. In Ref. 83 the contact diagrams with O_5 are given the main role in the explanation of the $\Delta I = 1/2$ rule, while in Ref. 76 it is asserted that the contribution of $M_{O_1-O_4}$ and M_{O_5} are negligibly small compared with the contribution from the pole dia-

TABLE XII. Widths of the decays $K \to 2\pi$ and $K \to 2\gamma$.

Approach	$\Gamma(K_S^0 \to \pi^+\pi^-)$, 10^{-15} GeV	$\Gamma(K^+ \to \pi^+\pi^0)$, 10^{-17} GeV	$\Gamma(K_L^0 \to \gamma\gamma)$, 10^{-23} GeV	$\Gamma(K_S^0 \to \gamma\gamma)$, 10^{-20} GeV
Model of chiral quark loops (Ref. 76)	5.94	1.8	6.7	1.75
MIT model (Ref. 78)	5.14	1.27	—	—
Harmonic-oscillator method (Ref. 78)	6,27	1.14		
Vacuum-insertion model (Ref. 83)	4.98	0.21		
Current-algebra methods with continuation to the physical region (Ref. 82)	5.11	1.12	—	—
$1/N_c$ expansion (Ref. 80)	5.34	1.89	6.26	—
Model with new neutral interaction (Ref. 86)	5.58	2.19	—	—
Method of chiral Lagrangians (Ref. 74)	4.85	—	—	—
QCM	5.38	1.24	7.18	1.53
Experiment	5.06±0.03 (Ref. 38)	1.13±0.01 (Ref. 38)	7.68±0.21 (Ref. 95)	1.84±0.92 (Ref. 95)

TABLE XIII. Relative contributions to the $K_S^0 \to \pi^+\pi^-$ decay amplitude.

$M(K_S^0 \to \pi^+\pi^-)$	$\frac{M_{O_1 - O_4}}{M}$	$\frac{M_{O_5}}{M}$	$\frac{M^{\varepsilon}_{O_5}}{M}$
$38.2 \cdot 10^{-8}$ GeV	0.23	0.02	0.75

gram with the intermediate ε meson. On the other hand, in Ref. 79 it is shown that the contribution from O_5, with allowance for the pole terms, is only about 10% and that the operators O_1–O_5 play the main part. It can be seen from Table XIII that in the QCM all three contributions to $M(K_S^0 \to \pi^+\pi^-)$ are important. The enhancement of the $\Delta I = 1/2$ amplitude due to the operators O_1–O_4 is associated with the coefficients c_1–c_4, and the important contribution from O_5 is associated with the intermediate ε meson.

Thus, it can be assumed that the intermediate scalar meson $\varepsilon(600)$ plays the main role in the explanation of the $\Delta I = 1/2$ rule.

We are very grateful to N. N. Achasov, S. B. Gerasimov, A. B. Govorkov, Yu. A. Gol'fand, M. K. Volkov, A. V. Efremov, B. L. Ioffe, L. G. Landsberg, D. Nardulli, V. A. Petrun'kin, and E. P. Shabalin for fruitful discussions and helpful comments.

[1]H. B. Nielsen, Preprint NBI-HE-87-61 (1987).
[2]M. A. Shifman, A. I. Vainshtein, and V. I. Zakharov, Nucl. Phys. **B147**, 385 (1979).
[3]P. N. Bogolyubov and A. E. Dorokhov, Fiz. Elem. Chastits At. Yadra **18**, 917 (1987) [Sov. J. Part. Nucl. **18**, 391 (1987)].
[4]E. Witten, Nucl. Phys. **B223**, 422 (1983).
[5]I. Gasser and M. Leutwyler, Ann. Phys. (N.Y.) **158**, 142 (1984).
[6]N. I. Karchev and A. A. Slavnov, Teor. Mat. Fiz. **65**, 192 (1985).
[7]A. A. Andrianov and Yu. V. Novozhilov, Phys. Lett. **153B**, 422 (1985).
[8]Y. Nambu and G. Jona-Lasinio, Phys. Rev. **122**, 345 (1961).
[9]T. Eguchi, Phys. Rev. D **14**, 2755 (1976).
[10]T. Goldman and R. W. Haymaker, Phys. Rev. D **24**, 724 (1981).
[11]M. K. Volkov, Fiz. Elem. Chastits At. Yadra **17**, 433 (1986) [Sov. J. Part. Nucl. **17**, 186 (1986)].
[12]H. Leutwyler, Nucl. Phys. **B179**, 129 (1981).
[13]E. V. Shuryak, Phys. Rep. **115**, 151 (1984).
[14]D. I. Dyakonov and V. Yu. Petrov, Nucl. Phys. **B245**, 259 (1984).
[15]S. G. Matinyan and G. K. Savvidy, Nucl. Phys. **B134**, 539 (1978).
[16]J. Ambjorn, N. K. Nielsen, and P. Olesen, Nucl. Phys. **B152**, 75 (1979).
[17]J. Finjord, Nucl. Phys. **B194**, 77 (1982).
[18]G. 't Hooft, Phys. Rev. D **14**, 3432 (1976).
[19]R. D. Carlitz and D. B. Creamer, Ann. Phys. (N.Y.) **118**, 429 (1979).
[20]C. G. Callan, R. Dashen, and D. J. Gross, Phys. Rev. D **17**, 2717 (1978); **19**, 1826 (1979).
[21]J. F. Donoghue, E. Golowich, and B. Holstein, Phys. Rep. **131**, 319 (1986).
[22]L. D. Faddeev and A. A. Slavnov, *Gauge Fields: Introduction to Quantum Theory* (Benjamin/Cummings, Reading, Mass., 1980) [Russ. original, 2nd ed., Nauka, Moscow, 1988].
[23]A. Dhar, R. Shanhar, and S. R. Wadia, Phys. Rev. D **31**, 3256 (1985).
[24]K. Hayashi, M. Hirayama, T. Muta *et al.*, Fortschr. Phys. **15**, 625 (1967).
[25]G. V. Efimov and M. A. Ivanov, Fiz. Elem. Chastits At. Yadra **12**, 1220 (1981) [Sov. J. Part. Nucl. **12**, 489 (1981)].
[26]G. V. Efimov, *Nonlocal Interactions of Quantized Fields* [in Russian] (Nauka, Moscow, 1977).
[27]G. V. Efimov, M. A. Ivanov, and V. E. Lyubovitskiĭ, Preprint R2-87-776 [in Russian], JINR, Dubna (1987).
[28]S. Gasiorowicz, *Elementary Particle Physics* (Wiley, New York, 1966) [Russ. transl., Nauka, Moscow, 1969].
[29]V. de Alfaro *et al.*, *Currents in Hadron Physics* (North-Holland, Amsterdam, 1973) [Russ. transl., Mir, Moscow, 1976].
[30]Ta-Pei Cheng and Ling-Fong Li, *Gauge Theory of Elementary Particle Physics* (Clarendon Press, Oxford, 1984) [Russ. transl., Mir, Moscow, 1987].
[31]L. G. Landsberg, Usp. Fiz. Nauk **146**, 185 (1985) [Sov. Phys. Usp. **28**, 435 (1985)].
[32]J. Fischer, P. Extermann, O. Guisan *et al.*, Phys. Lett. **73B**, 359 (1978).
[33]R. I. Dzhelyadin, S. V. Golovkin, V. A. Kachanov *et al.*, Phys. Lett. **94B**, 548 (1980).
[34]R. I. Dzhelyadin, S. V. Golovkin, and A. S. Konstantinov, Phys. Lett. **102B**, 296 (1981).
[35]J. Fischer, P. Extermann, O. Guisan *et al.*, Phys. Lett. **73B**, 364 (1978).
[36]R. I. Dzhelyadin, S. V. Golovkin, V. A. Kachanov *et al.*, Phys. Lett. **97B**, 471 (1980).
[37]B. L. Young, Phys. Rev. **161**, 1620 (1967).
[38]Particle Data Group, Phys. Lett. **170B**, 169 (1986).
[39]M. F. Heyn and C. B. Lang, Z. Phys. C **7**, 169 (1981).
[40]L. M. Barkov, A. V. Chilingarov, S. I. Eidelman *et al.*, Nucl. Phys. **B256**, 365 (1985).
[41]D. Bisello, Preprint LAL/85-15, Orsay (1985).
[42]S. R. Amendolia, M. Arik, B. Badelek *et al.*, Nucl. Phys. **B277**, 168 (1986).
[43]A. V. Radyushkin, Acta Phys. Pol. **B15**, 403 (1984).
[44]C. J. Bebek, C. N. Brown, S. D. Holmes *et al.*, Phys. Rev. D **17**, 1693 (1978).
[45]S. Dubnička, V. A. Meshcheryakov, and J. Milko, J. Phys. G **7**, 605 (1981).
[46]A. S. Vodop'yanov and É. N. Tsyganov, Fiz. Elem. Chastits At. Yadra **15**, 5 (1984) [Sov. J. Part. Nucl. **15**, 1 (1984)].
[47]P. Estabrooks and A. D. Martin, Nucl. Phys. **B79**, 301 (1974).
[48]S. D. Protopopescu, M. Alston-Garnjost, A. Barbaro-Galtieri *et al.*, Phys. Rev. D **7**, 1279 (1973).
[49]E. A. Alekseeva, A. A. Kartamyshev, V. K. Makar'in *et al.*, Zh. Eksp. Teor. Fiz. **82**, 1007 (1982) [Sov. Phys. JETP **55**, 591 (1982)].
[50]A. Stetz, J. Carroll, D. Ortendahl *et al.*, Nucl. Phys. **B138**, 285 (1978).
[51]A. Bay, D. Rüegger, B. Gabiond *et al.*, Phys. Lett. **174B**, 445 (1986).
[52]S. Egly, R. Engfer, Ch. Grab *et al.*, Phys. Lett. **175B**, 97 (1986).
[53]L. E. Pilonen, R. D. Bolton, M. D. Cooper *et al.*, Phys. Rev. Lett. **57**, 1402 (1986).
[54]C. A. Dominguez and J. Sola, Phys. Lett. **208B**, 131 (1988).
[55]D. A. Brymon, P. Depomier, and C. Leroy, Phys. Rep. **68**, 151 (1982).
[56]C. Y. Lee, Phys. Rev. D **32**, 658 (1985).
[57]N. Paver and M. D. Scadron, Nuovo Cimento **78A**, 159 (1983).
[58]A. N. Ivanov, M. Nagy, and M. K. Volkov, Phys. Lett. **200B**, 171 (1988).
[59]E. Z. Avakyan, S. L. Avakyan, G. V. Efimov, and M. A. Ivanov, Yad. Fiz. **46**, 576 (1987) [Sov. J. Nucl. Phys. **46**, 317 (1987)].
[60]A. B. Govorkov, Z. Phys. C **32**, 405 (1986).
[61]J. A. Dankowych, P. Brockman, K. W. Edwards *et al.*, Phys. Rev. Lett. **46**, 580 (1981).
[62]E. P. Shabalin, Yad. Fiz. **40**, 262 (1984) [Sov. J. Nucl. Phys. **40**, 166 (1984)].
[63]N. N. Achasov, S. A. Devyanin, and G. N. Shestakov, Usp. Fiz. Nauk **142**, 361 (1984) [Sov. Phys. Usp. **27**, 161 (1984)].
[64]J. Ellis and J. Lanik, Phys. Lett. **175B**, 83 (1983).
[65]O. Dumbrajs, R. Koch, H. Pilkuhn *et al.*, Nucl. Phys. **B216**, 277 (1983).
[66]A. A. Bel'kov and S. A. Bunyatov, Fiz. Elem. Chastits At. Yadra **13**, 5 (1982) [Sov. J. Part. Nucl. **13**, 1 (1982)].
[67]S. Weinberg, Phys. Rev. Lett. **17**, 616 (1966).
[68]L. L. Nemenov, Yad. Fiz. **41**, 980 (1985) [Sov. J. Nucl. Phys. **41**, 629 (1985)].
[69]S. M. Bilen'kiĭ, Nguyen Van Hieu, L. L. Nemenov, and F. G. Tkebuchava, Yad. Fiz. **10**, 812 (1969) [Sov. J. Nucl. Phys. **10**, 469 (1970)].
[70]G. V. Efimov, M. A. Ivanov, and V. E. Lyubovitskiĭ, Yad. Fiz. **44**, 460 (1986) [Sov. J. Nucl. Phys. **44**, 296 (1986)].
[71]G. Feinberg and J. Sucher, Phys. Rev. A **2**, 2395 (1970).
[72]M. V. Terent'ev, Usp. Fiz. Nauk **112**, 37 (1974) [Sov. Phys. Usp. **17**, 20 (1975)].
[73]V. A. Petrun'kin, Fiz. Elem. Chastits At. Yadra **12**, 692 (1981) [Sov. J.

Part. Nucl. **12**, 278 (1981)].
[74]E. Goudagini, Phys. Scr. **27**, 69 (1983).
[75]A. M. Vaĭnshteĭn, V. I. Zakharov, and M. A. Shifman, Zh. Eksp. Teor. Fiz. **72**, 1275 (1977) [Sov. Phys. JETP **45**, 670 (1977)].
[76]M. K. Volkov, A. N. Ivanov, and N. I. Troitskaya, Yad. Fiz. **47**, 1157 (1988) [Sov. J. Nucl. Phys. **47**, 736 (1988)].
[77]J. F. Donoghue and E. Golowich, Phys. Rev. D **14**, 1386 (1976).
[78]P. Colic and J. Trampetic, Phys. Rev. D **26**, 2286 (1982).
[79]G. Nardulli, Phys. Lett. **168B**, 120 (1986).
[80]A. J. Buras and J. M. Gerard, Nucl. Phys. **B264**, 371 (1986).
[81]W. A. Bardeen, A. J. Buras, and J.-M. Gérard, Phys. Lett. **180B**, 133 (1986).
[82]B. Guberina, D. Tadić, and J. Trampetić, Nucl. Phys. **B202**, 317 (1982).
[83]M. Milošević, D. Tadić, and J. Trampetić, Nucl. Phys. **B187**, 514 (1981).
[84]R. E. Shrock and S. B. Treiman, Phys. Rev. D **19**, 2148 (1979).
[85]C. T. Hill and G. G. Ross, Phys. Lett. **94B**, 234 (1980).
[86]H. Fusaoka, Prog. Theor. Phys. **62**, 554 (1979).
[87]E. B. Dally, J. M. Hauptman, J. Kubic *et al.*, Phys. Rev. Lett. **48**, 375 (1982).
[88]W. R. Molzon, J. Hoffnagle, J. Roehrig *et al.*, Phys. Rev. Lett. **41**, 1213 (1978).
[89]F. Dydak, C. Geweniger, F. L. Navarria *et al.*, Nucl. Phys. **B102**, 253 (1976).
[90]V. N. Bolotov, S. N. Gninenko, R. M. Dzhalkibaev *et al.*, Pis'ma Zh. Eksp. Teor. Fiz. **47**, 8 (1988) [JETP Lett. **47**, 7 (1988)].
[91]M. K. Volkov and A. A. Osipov, Yad. Fiz. **39**, 694 (1984) [Sov. J. Nucl. Phys. **39**, 440 (1984)].
[92]Yu. M. Antipov, V. A. Batarin, V. A. Bessubov *et al.*, Phys. Lett. **121B**, 445 (1983).
[93]V. V. Golubev, S. I. Dolinskiĭ, V. P. Druzhinin *et al.*, Yad. Fiz. **45**, 1004 (1987) [Sov. J. Nucl. Phys. **45**, 622 (1987)].
[94]P. Minkowski, BUTP-Preprint 84/30, Bern (1984).
[95]H. Burkhardt, P. Clarke, D. Cundy *et al.*, Phys. Lett. **199B**, 139 (1987).
[96]S. B. Gerasimov, Yad. Fiz. **29**, 513 (1979) [Sov. J. Nucl. Phys. **29**, 259 (1979)].
[97]J. Osson, in *Proc. of the 1987 Intern. Symposium on Lepton and Photon Interactions at High Energies, Hamburg, 27–31 July, 1987*, edited by W. Bartel and R. Ruckl (DESY, North-Holland, Hamburg–Amsterdam, 1987), p. 613.

Translated by Julian B. Barbour